

MACHINABILITY COMPARISON BETWEEN TWO TITANIUM ALLOYS

MACHINABILITY COMPARISON BETWEEN TWO DIFFERENT GRADES OF
TITANIUM ALLOYS UNDER DIVERSE TURNING AND COOLING
CONDITIONS:

Ti-6Al-4V and Ti-5Al-5V-5Mo-3Cr

By PIETRO STOLF, B. ENG.

A Thesis Submitted to the School of Graduate Studies in Partial Fulfillment of the
Requirements for the Degree Master of Applied Sciences

McMaster University © Copyright by Pietro Stolf, August 2019

McMaster University MASTER OF APPLIED SCIENCE (2019) Hamilton, Ontario
(Mechanical Engineering)

TITLE: Machinability Comparison Between Two Different Grades of Titanium Alloys Under Diverse Turning and Cooling Conditions: Ti-6Al-4V and Ti-5Al-5V-5Mo-3Cr AUTHOR: Pietro Stolf B. Eng., Mechanical Engineering SUPERVISOR: Dr. Stephen C. Veldhuis NUMBER OF PAGES: xv, 83.

ABSTRACT

The machining of a new alloy often presents a challenge. While useful assumptions can be drawn from materials of similar properties, there will always be unpredictable outcomes. Titanium alloys have been employed in the aerospace industry due to their high mechanical properties and good strength-to-weight ratio. Ti-64 (Ti-6Al-4V) was the standard choice until recently, when Ti-555.3 (Ti-5Al-5V-5Mo-3Cr) began to take its place. Ti-555.3 has improved resistance to fatigue and higher mechanical properties compared to Ti-64 and is able to maintain its strength when exposed to high temperatures, which warrants its acceptance for many applications. However, its chemical reactivity, low thermal conductivity and high mechanical properties are known to cause challenges when cutting this alloy. Making use of both experimental procedures and computational resources, this work presents a comparison between these two aerospace alloys under different process conditions, setting the ground for further academic development and optimization strategies. Determining that these alloys are substantially different from a machinability standpoint (lower tool life, abrasion & chipping as dominant wear mechanisms and nonuniform chip formation for Ti555.3 versus Ti-64). Based on this further investigation should be carried out for optimal tooling selection to improve the machining of Ti555.3.

ACKNOWLEDGEMENTS

Firstly, I gratefully acknowledge that this research was supported by the Natural Sciences and Engineering Research Council of Canada (NSERC) under the CANRIMT Strategic Research Network Grant NETGP 479639-15.

I would like to express my gratitude to Dr. Veldhuis, who has given me the opportunity to work at the MMRI and has provided me all the necessary resources to develop this research. I would also like to thank Dr. Paiva and Dr. Fox-Rabinovich, for their guidance and tutorship during these two years. They have played a role of utmost importance in the realization of this project. My thanks are also extended to my colleague and roommate, Edinei Locks Junior, who has assisted me numerous times during this period, in both technical and personal matters. In addition, I would like to express my deep appreciation for my laboratory colleagues, who have helped me with the analyses that made this work possible, as well as all my professors, who have shared with me a portion of their knowledge, which is now applied in this research.

Finally, special thanks to my wife, Mariana Silva de Lima, who was by my side and has given me her unconditional support during this journey, and to my parents who have believed in my potential and thoroughly invested in my education.

CONTENTS

ABSTRACT	iii
ACKNOWLEDGEMENTS	iv
LIST OF FIGURES.....	ix
LIST OF TABLES	xiii
NOMENCLATURE	xiv
1. Introduction	1
1.1. Background	1
1.2. Motivation	2
1.3. Thesis Outline.....	4
1.3.1. Chapter 2	4
1.3.2. Chapter 3	4
1.3.3. Chapter 4	4
1.3.4. Chapter 5	5
1.3.5. Chapter 6	5

1.3.6. Chapter 7	5
2. Literature review.....	6
2.1. Titanium Alloys	6
2.1.1. Classification.....	7
2.1.2. Machinability	8
2.1.3. Ti-6Al-4V	9
2.1.4. Ti-5Al-5V-5Mo-3Cr.....	15
2.2. High Pressure Coolant (HPC)	20
2.3. Finite Element Analysis (FEA).....	23
2.3.1. Formulation.....	24
2.3.2. Constitutive Model	25
2.3.3. Adaptive remeshing	26
3. Research Objectives and Methodology.....	27
3.1. Objectives.....	27
3.1.1. Specific objectives	27

3.2. Methodology	28
4. Materials and Methods.....	30
4.1. Finite Element Analysis (FEA).....	30
4.2. Experimental procedures.....	32
5. Results and Discussion: Ti-6Al-4V	37
5.1. Finite Element Analysis (FEA).....	37
5.2. Tool Life.....	40
5.3. Tool Wear Modes and Mechanisms	44
5.4. Chip Analysis.....	47
6. Results and Discussion: Ti-5Al-5V-5Mo-3Cr.....	53
6.1. Finite Element Analysis (FEA).....	53
6.2. Tool Life.....	58
6.3. Tool Wear Modes and Mechanisms	60
6.4. Chip Analysis.....	63
7. Conclusions	70

8. References..... 74

LIST OF FIGURES

Figure 1: Titanium phase diagram [18].....	8
Figure 2: Chip shear deformation zones [4].....	14
Figure 3: Chip shear deformation zones for Ti-5553 [4].	19
Figure 4: Graphic representation highlighting the changes in chip formation and contact length between (a) flood/dry and (b) HPC conditions.....	22
Figure 5: Experimental/FEA summary.....	29
Figure 6: FEA model domain	32
Figure 7: (a) Machine tool, (b) workpiece, dynamometer, tool holder setup and (c) detailed view of tool and coolant-through tool holder.....	34
Figure 8: Experimental temperature measurement point.....	35
Figure 9: Temperature measurements for both simulation and experimental conditions of Ti-6Al-4V combined with FEA results for chip formation at (a,d) flood – 150 m/min, (b,e) 1000 psi – 150 m/min and (c,f) 1000 psi – 250 m/min.	38
Figure 10: Tool stress profiles and TCCL for Ti-6Al-4V at (a) flood – 150 m/min, (b) 1000 psi – 150 m/min and (c) 1000 psi – 250 m/min.	39

Figure 11: Flank wear comparison chart + MRR values for all conditions of Ti-6Al-4V.....	41
Figure 12: Tool wear progression curves for Ti-6Al-4V at flood – 150 m/min, 1000 psi – 150 m/min and 1000 psi – 250 m/min.	42
Figure 13: Cutting forces for Ti-6Al-4V at flood – 150 m/min, 1000 psi – 150 m/min and 1000 psi – 250 m/min.	43
Figure 14: FEA cutting forces for flood – 150 m/min.....	44
Figure 15: SEM of worn inserts for Ti-6Al-4V at (a) flood – 150 m/min, (b) 1000 psi – 150 m/min and (c) 1000 psi – 250 m/min, indicating the presence of oxidation, crater, BUE and flank wear modes.	45
Figure 16: Volumetric analysis of worn tools for Ti-6Al-4V at (a) flood – 150 m/min, (b) 1000 psi – 150 m/min and (c) 1000 psi – 250 m/min, indicating the volumes of adhered and removed material from the cutting inserts.....	46
Figure 17: SEM of (a) chip undersurfaces and (b) shear bands for Ti-6Al-4V.	48
Figure 18: Tribological conditions along the rake face of the insert for Ti-6Al-4V at (a) dry / flood, and (b) high-pressure coolant conditions.....	49
Figure 19: Chips cross-sections and EBSD orientation maps for Ti-6Al-4V at (a,b) flood – 150 m/min, (c,d) 1000 psi – 150 m/min and (e,f) 1000 psi – 250 m/min.	50

Figure 20: Chips shear bands microhardness values for Ti-6Al-4V at flood – 150 m/min, 1000 psi – 150 m/min and 1000 psi – 250 m/min with the points located near the tool-chip interface highlighted. 52

Figure 21: Temperature measurements for both simulation and experimental conditions of Ti-5Al-5V-5Mo-3Cr combined with FEA results for chip formation at (a,c) flood – 150 m/min, (b,d) 1000 psi – 40 m/min, (e,g) 1000 psi – 150 m/min and and (f,h) 1000 psi – 250 m/min. 55

Figure 22: Tool stress profiles and TCCL for Ti-5Al-5V-5Mo-3Cr at (a) flood – 150 m/min, (b) 1000 psi – 40 m/min, (c) 1000 psi – 150 m/min and (d) 1000 psi – 150 m/min. 57

Figure 23: Tool wear progression curves for Ti-5Al-5V-5Mo-3Cr at flood – 150 m/min, 1000 psi – 40 m/min, 1000 psi – 150 m/min and 1000 psi – 250 m/min for (a) long and (b) short passes. 59

Figure 24: Cutting forces for Ti-5Al-5V-5Mo-3Cr at flood – 150 m/min, 1000 psi – 40 m/min, 1000 psi – 150 m/min and 1000 psi – 250 m/min. 60

Figure 25: SEM of worn inserts of Ti-5Al-5V-5Mo-3Cr at (a) flood – 150 m/min, (b) 1000 psi – 40 m/min, (c) 1000 psi – 150 m/min and (d) 1000 psi – 250 m/min, indicating the presence of oxidation, edge chipping, BUE and flank wear modes. 62

Figure 26: Volumetric analysis of worn tools for Ti-5Al-5V-5Mo-3Cr at (a) flood – 150 m/min, (b) 1000 psi – 40 m/min, (c) 1000 psi – 150 m/min and (d) 1000 psi – 250 m/min, indicating the volumes of adhered and removed material from the cutting inserts. 63

Figure 27: SEM of (a) chip undersurfaces and (b) shear bands for Ti-5Al-5V-5Mo-3Cr..... 65

Figure 28: Tribological conditions along the rake face of the insert for Ti-5Al-5V-5Mo-3Cr at high-pressure coolant conditions. 66

Figure 29: EBSD orientation maps for Ti-6Al-4V at (a) flood – 150 m/min, (b) 1000 psi – 40 m/min, (c) 1000 psi – 150 m/min and (d) 1000 psi – 150 m/min. 67

Figure 30: Microhardness values for Ti-5Al-5V-5Mo-3Cr at flood – 150 m/min, 1000 psi – 40m/min, 1000 psi – 150 m/min and 1000 psi – 250 m/min with points located near the tool-chip interface highlighted..... 69

LIST OF TABLES

Table 1: Chemical composition of Ti-6Al-4V at room temperature according to the supplier.....	10
Table 2: Mechanical properties of Ti-6Al-4V at room temperature according to the supplier.....	11
Table 3: Chemical composition of Ti-5Al-5V-5Mo-3Cr at room temperature according to the supplier.....	15
Table 4: Mechanical properties of Ti-5Al-5V-5Mo-3Cr at room temperature according to the supplier.....	16
Table 5: Simulation parameters for all the tested conditions.	31
Table 6: Machining parameters for experimental testing.	33
Table 7: Chips shear bands microhardness profiles for Ti-6Al-4V at flood – 150 m/min, 1000 psi – 150 m/min and 1000 psi – 250 m/min with values highlighted for the points located near the tool-chip interface.	51
Table 8: Chips shear bands microhardness profiles for Ti-5Al-5V-5Mo-3Cr at flood – 150 m/min, 1000 psi – 40 m/min, 1000 psi – 150 m/min and 1000 psi – 250 m/min with values highlighted for points located near the tool-chip interface.	68

NOMENCLATURE

Ti-64 – Ti-6Al-4V

Ti-555.3 – Ti-5Al-5V-5Mo-3Cr

MMRI – McMaster Manufacturing Research Institute

ACARE – Advisory Council for Aviation Research in Europe

MRR – Material Removal Rate

HPC – High-Pressure Coolant

CP – Commercially Pure

HCP – Hexagonal Close-Packed

BCC – Body-Centered Cubic

UTS – Ultimate Tensile Strength

BUE – Built-Up Edge

MQL – Minimum Quantity Lubrication

TCCL – Tool-Chip Contact Length

FEA – Finite Element Analysis

PDE – Partial Differential Equation

SEM – Scanning Electron Microscopy

EBSB – Electron Backscatter Diffraction

CAE – Computer-Aided Engineering

CNC – Computer Numerical Control

EDM – Electrical Discharge Machining

SE – Secondary Electron

V_p – Volume of peaks above reference

V_v – Volume of valleys below reference

SSDZ – Secondary Shear Deformation Zone

V_c – Cutting speed

DOC – Depth of Cut

1. Introduction

The development and performance optimization of new alloys has been continuous throughout history. Industry sets high demands for technologies aimed at cost reduction, meeting market requirements and regulatory compliance and overcoming competition. All these concerns have been directed towards the academic community, fueling scientific discoveries. Each newly released material developed still requires processing to realize a final product. Thus, a change generates a chain reaction every time a new alloy composition is revealed to the public. All data gathered of a material's processing characteristics will also contribute to the broadening of its application range and productivity level.

1.1. Background

Ti-6Al-4V, also known as Ti-64, is the titanium alloy with the broadest range of applications, that accounts for 45-65% of the world's titanium consumption [1]–[3]. It is widely employed in the aerospace industry, mainly due to its exceptional specific strength and unmatched mechanical properties [1], [2], [4]. The applications range from engines to structural parts such as landing gear. In recent times, the aerospace industry has been tasked to overcome new challenges

regarding the efficiency of newly manufactured aircrafts. The “Flightpath 2050” long term agreement, established by the Advisory Council for Aviation Research in Europe (ACARE) [5] is a perfect example of these changes. Weight and noise reduction as well as fuel consumption are some of the targeted aspects. These challenges have stimulated the search for alternate “optimized” materials that offer improved mechanical properties and resistance to higher operating temperatures, such as Ti-555.3 (Ti-5Al-5V-5Mo-3Cr) [6], [7]. Compared to Ti-64, Ti-555.3 offers improved resistance to fatigue, higher ultimate tensile strength, higher yield strength and can retain its strength at high temperatures [7]–[9]. However, the high levels of chemical reactivity and low thermal conductivity of this material inhibits its machinability, thus earning its classification among difficult-to-cut materials [9]–[11]. The combination of these aspects will result in rapid tool wear, low Material Removal Rate (MRR) and ultimately, low productivity indexes.

1.2. Motivation

Previous research [4], [6]–[9] has already addressed the advantages of implementing near- β titanium alloys in aerospace applications. However, these same studies also outline its machinability problems, such as short tool life and poor chip control.

The extensive database available on tool wear, chip formation and coolant application of Ti-64 can become a powerful tool for uncovering the yet unknown characteristics of Ti-555.3. A comparison under different process conditions can also provide meaningful data that will fill some of the gaps in the current research which comprise the turning of Ti-555.3 under wet conditions and its influence in wear mechanisms, chip formation and tool life, thus providing the grounds for further academic study.

For reliable performance to be obtained, different cooling strategies must be taken into consideration. Therefore, the efficiency of a High-Pressure Coolant (HPC) supply is evaluated in this work by comparing the tool life, cutting forces, wear mechanisms and chip formation under different cutting conditions in both studied alloys. At high cutting speeds, heat becomes the main source of accelerated tool wear. Use of HPC reduces thermal and mechanical loads making it ideal for the machining of titanium alloys [10]. The benefits of HPC have already been outlined for Ti-64 machining [12].

1.3. Thesis Outline

1.3.1. Chapter 2

This chapter provides an overview of previously published work relevant to the subject of this thesis. A summary of the current available knowledge is presented. This compilation of findings is used in the upcoming chapters to support the collected experimental data.

1.3.2. Chapter 3

This section establishes the main objective of this work in a procedural form. Items reported in the methodology section provide a list of experiments and analyses according to the procedures outlined in the next chapter.

1.3.3. Chapter 4

This chapter describes all experimental procedures at an appropriate level of detail. All operating parameters are disclosed to enable future repeatability of the obtained results. Equipment specifications are also presented in this section.

1.3.4. Chapter 5

The results obtained from cutting tests performed on Ti-6Al-4V are presented in this chapter. Data from previous research and the literature is used to corroborate this study's findings and accurately describe the phenomena that take place during the machining of this alloy.

1.3.5. Chapter 6

All results obtained from tests performed on Ti-5Al-5V-5Mo-3Cr are presented in this chapter. Findings are corroborated with data from literature to provide an accurate description of the phenomena that take place during the machining of this alloy.

1.3.6. Chapter 7

The final section of this research summarizes all important findings obtained throughout this work. A brief examination of results that fulfilled the initial objectives is provided, along with the subjects requiring further investigation.

2. Literature review

2.1. Titanium Alloys

Titanium alloys have become a subject of major interest since the late 1940's for high-strength / high-temperature applications [1].

Compared to other light-weight structural materials (e.g. aluminum), titanium's mechanical, thermal and chemical properties make it suitable for a wide variety of uses, with the added benefit of its considerably higher melting point [1], [13]–[15]. Although titanium is among the 4 most plentiful structural metals on earth, its high cost and challenging processing conditions limit its usage to high-end, low to medium scale production equipment, such as aerospace and biomedical components [1], [13], [14].

Titanium is currently being commercialized in both its pure form, also known as Commercially Pure (CP) and alloyed with other elements, which alter the material's thermal and mechanical properties according to the specific application [1]. Some of titanium's most desirable properties are: high strength-to-weight ratio, strength retention at high operating temperatures, a relatively low elastic modulus as well as high corrosion and fatigue resistance [1], [14], [15].

Use of titanium alloys in the aerospace industry falls into two categories: frames and engines. While Ti-6Al-4V still accounts for more than half of the world's titanium production, β alloys have gained more widespread use in recent years, mainly for structural aircraft components such as aero frames and landing gears. Although the extent of their use fluctuates from one manufacturer to another, there is a clearly growing demand for β titanium alloys in the aerospace industry [1], [16].

2.1.1. Classification

Titanium undergoes a phase transformation of an allotropic nature at 880°C [1], [9], [17]. At lower temperatures, its microstructure consists mostly of Hexagonal Close-Packed (HCP) crystals, also known as α phases. Once the recrystallization temperature is reached, the crystallographic structure shifts to a Body-Centred Cubic (BCC) form, also known as a β phase [1], [17]. However, this exact transformation temperature will only occur for 100% pure titanium samples. When working with titanium alloys, the presence of certain elements known as stabilizers, determines the alloy's dominant phase. As shown in figure 1, elements such as Molybdenum and Vanadium favor a BCC crystallographic structure, whereas Aluminum and Carbon will act as α stabilizers, making the HCP structure predominant [1], [18]. Such compositions are directly related to the material's ability to obtain ultimate tensile strength (UTS) and hardness (H), upon aging. Although

α titanium alloys present lower mechanical properties, their resistance to corrosion is superior compared to β alloys. [19], [20].

Near- β alloys composed of a β matrix with the presence of α precipitates incorporate high mechanical resistance characteristics provided by the β phase combined with the corrosion properties of α alloys [21]. Figure 1 presents the phase diagram and the positions of each of the alloys studied in this work.

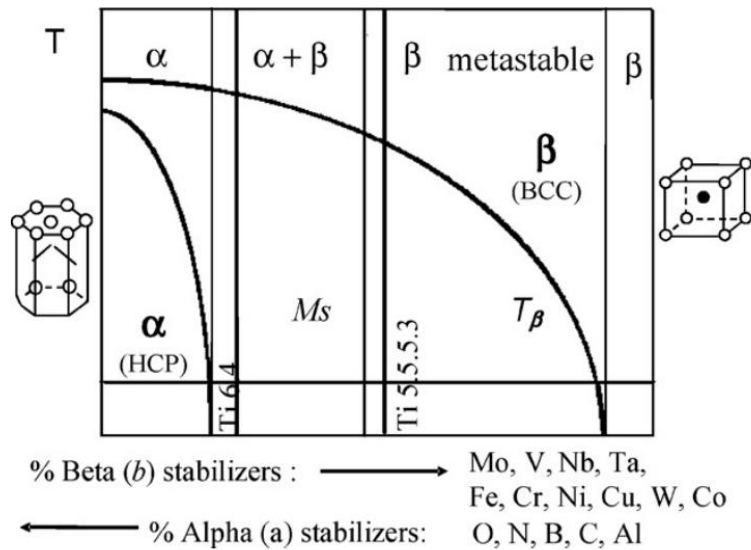


Figure 1: Titanium phase diagram [18]

2.1.2. Machinability

Titanium alloys' ability to be processed has not developed at the same rate as its alloys, which presents a major challenge for industrial research [22].

Due to titanium's low thermal conductivity, its ability to retain mechanical properties at high operating temperatures, high chemical reactivity and low elasticity modulus, these alloys are classified as difficult-to-cut materials [10], [11], [22]. Significant temperatures tend to be generated at the tool/chip interface during titanium machining, even at lower cutting speeds. Studies also show that the heat distribution during titanium alloy machining, differs greatly from that of other common structural materials. For example, when machining steel, 50% of the heat is expected to permeate into the cutting tool and the other 50% is absorbed by the chips and the workpiece. However, the amount of heat directed towards the tool reaches about 80% when machining titanium alloys on account of their low thermal conductivity. Cutting forces are reportedly similar to the values obtained for the machining of steel. Although, stress concentration near the cutting edge is notably higher [22], this could be due to a relatively small tool/chip contact length combined with titanium's high rates of work hardening [10].

2.1.3. Ti-6Al-4V

Since its introduction, Ti-6Al-4V is considered to be the most widespread $\alpha+\beta$ titanium alloy with the broadest range of applications, responsible for 45-65% of the world's titanium consumption [1]. Compared to other titanium alloys, such as near- α and β , Ti-64 provides a good compromise between strength, ductility,

fracture toughness, creep, processability, corrosion resistance and weldability, in addition to being able to be hardened and strengthened through heat treatment. For these reasons, Ti-64 is widely employed in the aerospace industry, especially for structural and “cooler” engine components, due to its moderate heat resistance, up to approximately 300°C. The latter property is highly dependant on the alloy’s β content [13]–[15].

Perhaps the biggest factor favoring the usage of Ti-64 would be the large body of information available on its treatment (annealing, quenching, aging) and processing methods, since this alloy’s capabilities have already been largely explored by industries and researchers over the years [23]. The composition and mechanical properties of the studied alloy are presented in tables 1 and 2.

Table 1: Chemical composition of Ti-6Al-4V at room temperature according to the supplier.

Al	V	Mo	Cr	Fe	Zr	C	O
5.5 - 6.75	3.5 - 4.5	---	---	0.4	---	0.1	0.2

Table 2: Mechanical properties of Ti-6Al-4V at room temperature according to the supplier.

Yield strength (MPa)	Tensile strength (MPa)	Elongation %	Hardness (HV)	Thermal conductivity (W/m·°C)	T_{melt} (°C)
828	895	10	360	6.6	1630

2.1.3.1. Machinability

In comparison to near- β and β titanium alloys, Ti-64 presents a relatively high machinability index, which is directly related to the tool's life span, due to its lower mechanical properties [4], [6], [9], [16], [21]. However, it is still classified as a difficult-to-cut material.

Highly concentrated cutting loads and temperatures, self excited vibrations and high chemical reactivity are the main factors that hinder the machinability of Ti-64. These will ultimately result in premature wear of the cutting tools and irregular chip formation [10], [22]. Therefore, the selection of appropriate tools and cutting parameters must take all these aspects into consideration.

2.1.3.1.1. Tool Wear

Diffusion and adhesion are the most important tool wear mechanisms encountered during Ti-64 machining [10], [16], [22]. The high temperatures

imposed on the cutting tool facilitate the diffusion process, generating crater wear mainly on the rake face of the inserts. Once crater wear reaches critical levels, it weakens the cutting tool's edge and directly affects the chip formation process, altering the tool-chip contact conditions [24]. Another outcome of the harsh processing conditions and Ti-64's reactivity with most available tools, is the strong adhesion of the workpiece material to the contact surfaces of the insert [22]. This phenomenon is usually intensified by the application of tool coatings, since the aluminum present in the alloy's composition tends to bond with the aluminum in the coating. The wear mode known as Built Up Edge (BUE) is a direct cause of the adhesion process. It consists of the accumulation of workpiece material on the tool's cutting edge, thus creating a "new" cutting surface. This type of wear is characterized by the irregularity and instability of the newly formed layer, which will directly affect the machined part's surface finish and dimensional accuracy [24].

Apart from diffusion and adhesion, abrasion is also present on the flank surface. However, this mechanism is inherent in the metal cutting process and is present in the machining of most alloys.

Based on the aforementioned wear mechanisms, the preferred tool choice for machining Ti-64 are uncoated carbide inserts, due to their solid combination of mechanical resistance, chemical inertness and thermal conductivity [22], [25].

2.1.3.1.2. Chip Formation

Segmented chips are a common outcome of titanium alloy machining. They are generated by instabilities in the chip formation process and consequent variation of axial force, which might impair the surface finish of the machined part and also induce the propagation of self-excited vibrations, known as chatter [10].

There exist three main theories concerning the chip formation process during the machining of Ti-based alloys [26], each relying on a different mechanism. The “Catastrophic Adiabatic Shear” theory states that deformation in the primary shear zone results in two distinct outcomes: work hardening and thermal softening. According to this theory, chip formation will only occur once the intensity of the thermal softening overcomes the work hardening phenomenon, thereby causing the material to fail. In the second theory, the propagation of cracks throughout the primary shear deformation zone is presumed to be the cause of separation. According to the third theory, plastic instabilities and localized strain are the two main factors that lead to catastrophic shear failure in the primary shear zone. A buildup of work material segments does not undergo sufficient deformation due to the flattening of the cutting edge, forming a so-called stagnation zone. When a previous segment begins to push against the next one, a ribbon-like structure is formed [26]. In figure 2, three zones can be identified in the chips generated by any metal cutting process [27]. The first one, known as the primary shear deformation

zone, consists of highly deformed alpha grains where maximum levels of shear stress are present during the cutting process. Similarly, the secondary shear deformation zone also contains highly deformed grains. However, these are oriented parallel to the tool's rake face. The highest temperatures are found in this region, facilitating the diffusion process that may lead to crater wear. Moreover, a third zone composed of non-distorted grains can be characterized in the middle of each serration.

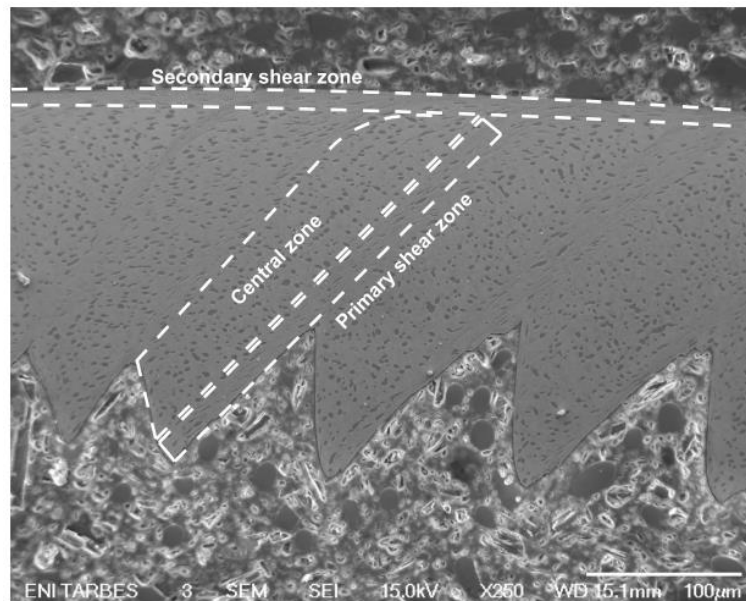


Figure 2: Chip shear deformation zones [4].

2.1.4. Ti-5Al-5V-5Mo-3Cr

Since Ti-5Al-5V-5Mo-3Cr or Ti-555.3 contains only 20% of the α phase, it is categorized as a near- β (β metastable) alloy [5], [9], [18], [21]. According to previous findings, Ti-555.3 has a similar Young's modulus compared to Ti-64. However, with a 30% higher yield and ultimate tensile strength as well as significantly lower ductility, these materials are substantially different from a mechanical standpoint [4], [18]. The equivalent Mo found in Ti-555.3 is considerably higher (approximately 8 times) than that of Ti-64, which partially accounts for its superior tensile load resistance [18]. All these properties translate into the material's ability to withstand higher workloads. However, they negatively impact its machinability [4], [8], [18]. Chemical composition and mechanical properties of the studied alloy are presented in tables 3 and 4 with values for Ti-64 repeated to aid comparison.

Table 3: Chemical composition of Ti-5Al-5V-5Mo-3Cr at room temperature according to the supplier.

	Al	V	Mo	Cr	Fe	Zr	C	O
Ti-64	5.5 - 6.75	3.5 - 4.5	---	---	0.4	---	0.1	0.2
Ti-555.3	4.4-5.7	4.0 - 5.5	4.0 - 5.5	2.5 - 3.5	0.3 - 0.5	0.3	0.1	0.2

Table 4: Mechanical properties of Ti-5Al-5V-5Mo-3Cr at room temperature according to the supplier.

Material	Yield strength (MPa)	Tensile strength (MPa)	Elongation %	Hardness (HV)	Thermal conductivity (W/m·°C)	T_{melt} (°C)
Ti-64	828	895	10	360	6.6	1630
Ti-555.3	1170	1290	6	415	5	1650

2.1.4.1. Machinability

Few studies have been conducted on the machinability of Ti-555.3. Therefore, critical aspects of its machining performance will be further explored in the results section.

Ti555.3 has an approximately 50% lower machinability index than Ti-64. While the wear modes and mechanisms as reported in the literature are similar in both alloys, their propagation rates and intensity are characterized as notably higher in Ti-555.3, indicating that its composition and microstructural differences have an effect on the cutting process [4], [18]. In addition, results obtained from the turning of Ti-555.3 show a pronounced temperature rise at the interface, in contrast to minimal temperature variation in the primary shear deformation zone. This is caused by the material's low thermal properties [4], [5], [8], [18]. Analytical data and experimental results provided evidence for an inverse relation between

temperature and coefficient of friction at the tool's rake face, which can be attributed to the accumulation of built up work material that forms an irregular contact surface [4], [10].

The chip formation process also reflects this alloy's poor machinability, with the appearance of adiabatic shear bands at a high frequency that might lead to fluctuations in cut and feed forces, which are considerably higher for the near- β alloy [18].

2.1.4.1.1. Tool Wear

Tests were performed on Ti-555.3 in previous studies with TiAlN coated carbide tools under dry turning conditions [4]. During these tests, tool wear was found to progress in three distinct stages. Diffusion and adhesion were reported to be the most active wear mechanisms that caused the deterioration of the tool rake face (crater wear) and further cutting-edge failure. Diffusion is a well-known phenomenon in titanium machining. It is generated by high thermal loads on the tool during the cutting process [10], [22]. TiAlN coatings were reported to fully detach after only 20% of the tool's life [4], due to the severe friction conditions at the tool/chip interface. This supports the current observation that uncoated grade k carbide tools are still the best option for the machining of Titanium alloys [22], [25]. Cutting force results show that during the final stages of the tool's life, the feed

forces begin to overcome the cutting forces, revealing a possible change in the rake angle due to material build up at the rake face of the tool. This theory was further confirmed by optical interferometry images [4].

2.1.4.1.2. Chip Formation

Two distinct regions can be noted [4], [28] on the undersurface of the chips obtained by Ti-555.3 machining. One is heavily segmented and the other is smoother with minimal presence of lamellar structures. The first region is generated by the straight section of the cutting edge, where chip thickness becomes maximum and instabilities arise. The second one is the result of the tool's nose radius, where cutting becomes more stable due to the smaller chip thickness [4].

In Ti-555.3 machining, some differences can be noted from the pattern pictured in figure 2. Wagner et al. reported two types of α nodules in the primary shear deformation zone (figure 3). The plane is composed of both highly and slightly deformed grains, which can be the result of the material's heterogeneity [4] and may also create additional process instabilities.

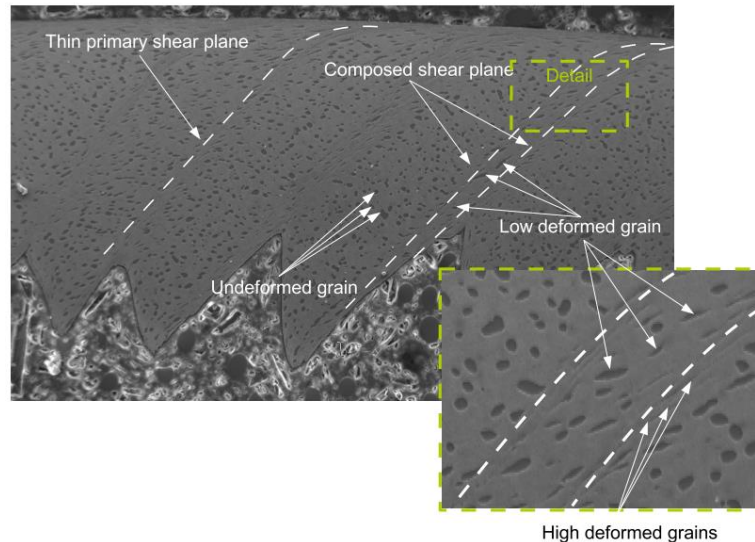


Figure 3: Chip shear deformation zones for Ti-5553 [4].

It was reported that changes in cutting speed will impact chip thickness. With higher speeds, chip segmentation depth is increased, thus reducing its minimum thickness. It is suggested that such alterations will act in favor of high-pressure cutting fluid application, granting the coolant's access to a region closer to the cutting edge. For Ti-555.3, as tool wear progresses, three distinct chip geometries were described [4]. At first, regular segmented chips are produced, with a homogenous geometry and repeated structure. When the tool becomes worn, two alternate segments are detected, the first is similar to the ones obtained in the first stage and a second smaller one. This behavior is explained by the authors as a consequence of the high deformation and temperature conditions, causing a high energy concentration that induces the appearance of a second primary shear

deformation zone [4]. Finally, the smaller segments disappear, and chip thickness is reduced due to BUE formation and the ensuing change in tool geometry. According to previous research, rake angle changes considerably throughout the machining process [1].

2.2. High Pressure Coolant (HPC)

Use of cutting fluids to reduce thermal and mechanical loads is a widespread technique for machining materials that have low thermal conductivity [10], [24], [29] which considerably reduces the appearance of thermal related wear phenomena, such as diffusion and adhesion, specially when compared to dry cutting. However, conventional coolant supplies do not ensure targeted fluid delivery in the cutting zone due to the sticking-sliding nature of the chip formation process [24], rendering inefficient coolant application by traditional methods [30]. Through careful setup, cutting fluids can be directed towards the primary, secondary and tertiary shear deformation zones. The secondary shear deformation zone, located at the tool/chip interface, exhibits a combination of high shear and normal stresses parallel to the tool/workpiece contact surface [24], [29]. It comprises the most heat intensive region during the cutting process that necessitates substantial cooling activity. However, flood coolant supplies cannot adequately access the secondary shear deformation zone, due to the vapour

barrier imposed by the severe tool/chip contact conditions, thereby preventing heat exchange between the cutting fluid and the cutting insert. To address this issue, different cooling strategies have been employed to improve the machining performance of titanium alloys. Cryogenic cooling was found to be a suitable alternative to conventional flood coolant supply when working with low thermal conductivity alloys [31]–[33]. Conversely, the use of cryogenic cooling significantly increases workpiece material hardness, negatively impacting mechanical loads and promoting accelerated tool wear rates in Ti alloys [30]. In addition to its high operational costs and impact on dimensional control, this makes cryogenic machining unfit for industrial applications involving titanium. The application of Minimum Quantity Lubrication (MQL) in titanium alloy machining was demonstrated to not be effective [31], [32], [34], [35], since its cooling capabilities are limited when dealing with the high levels of heat imposed by the cutting process.

One promising alternative emerging in this direction is the use of High-Pressure Coolant (HPC), which can address most of the aforementioned issues at a relatively low cost [30], [36], [37]. Moreover, the added benefit of using HPC for the machining of Ti alloys is an improved surface integrity [30]. Figure 4 illustrates some of the key benefits provided by the application of HPC to the rake face of the cutting tool. This includes the reduction of chip curl and promotion of chip

breakability from the additional applied bending moment as well as more effective heat dissipation from the tool-chip interface once the coolant reaches deep into the cutting zone [24], [38]. The shorter Tool-Chip Contact Length (TCCL) also contributes to lower diffusion wear rates and consequently prolongs the lifespan of the cutting tool [24], [38].

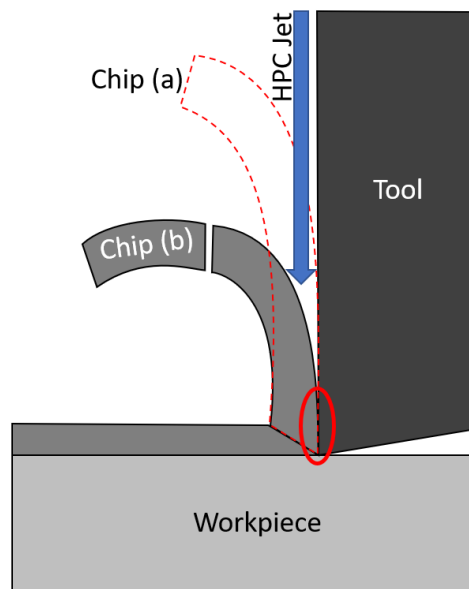


Figure 4: Graphic representation highlighting the changes in chip formation and contact length between (a) flood/dry and (b) HPC conditions.

2.3. Finite Element Analysis (FEA)

Computational simulations reduce the amount of physical experimentation needed for a process analysis scenario, enabling the user to narrow down its set of parameters before proceeding to the actual testing. Moreover, simulations also provide a wide range of data that would not otherwise be readily available.

The Finite Element Method (FEM) is a numerical technique for the approximation of results based on partial differential equations (PDE's). In this process, a physical domain is distributed into several subdomains, also known as elements, from which the results are then individually calculated. The determination of boundary conditions makes it possible to integrate these elements into a major solution. The number of elements to be calculated is defined by mesh convergence criteria, which establishes acceptable levels of result divergences at different degrees of mesh refinement. When setting up a simulation, the material model as well as the solution method need to be defined based on the nature and complexity of the proposed problem [39], [40].

The finite element analysis (FEA) is an essential tool for the evaluation of cutting conditions, such as temperature/stress profiles within the cutting zone. The primary difficulty in the FEA of metal cutting is capturing the severe plastic

deformation of the metal, which results in extreme tribological conditions at the tool-workpiece interface [41].

Modeling of metal turning requires a thorough understanding of the deformation conditions in the relevant deformation zones, strain rates, as well as the frictional conditions at the tool-workpiece interface. The cutting temperature/stress profile is critical for achieving control of the machining process [42]–[44].

2.3.1. Formulation

The numerical analyses in this work were carried out on a commercial FEA code (Thirdwave's Advantedge CAE software). Advantedge uses a Lagrangian approach combined with adaptive remeshing capabilities [40], [45], mainly due to the fact that a pure Lagrangian mesh would undergo significant levels of distortion, specially near the primary and secondary shear deformation zones. Hence, this formulation is responsible for addressing the non-linearities caused by the high levels of plastic deformation, strain rates and inherent resolution issues that emerge during the turning process. Refer to Man et al. [46] for additional details.

2.3.2. Constitutive Model

The constitutive model derived from the Cuitino and Ortiz stress update method is employed for the flow stress calculations (eq. 1), where $g(\alpha)$ refers to the strain hardening, $\Theta(T)$ to the thermal softening and $\Gamma(\dot{\alpha})$, α , $\dot{\alpha}$, and T refer to rate sensitivity, equivalent plastic strain, plastic strain rate, and temperature, respectively [46].

$$\sigma(\alpha, \dot{\alpha}, T) = g(\alpha)\Theta(T) \Gamma(\dot{\alpha}) \quad (1)$$

Furthermore, the power law (eq. 2) is used to describe strain hardening and rate sensitivity, where reference values for strain and strain rates are denoted by α_0 and $\dot{\alpha}_0$, respectively.

$$g(\alpha) = \left(\sigma_0 \left(1 + \frac{\alpha}{\alpha_0}\right)^{\frac{1}{N}}\right), \Gamma(\dot{\alpha}) = \left(1 + \frac{\dot{\alpha}}{\dot{\alpha}_0}\right)^{\frac{1}{M}} \quad (2)$$

A fifth order polynomial function is used to determine thermal softening (eq. 3) [46].

$$\Theta(T) = c_0 + c_1 T + \dots + c_5 T^5 \quad (3)$$

2.3.3. Adaptive remeshing

Adaptive remeshing enables the model to account for the element deformations intrinsic to the Lagrangian method. Deformations are being constantly monitored. Anytime a certain tolerance was met, refinement/coarsening algorithms were applied in to regenerate the mesh in the most optimal way [46]. The biggest advantage of this approach is the ability to resolve different scaled regions at different moments in time. Elements present in a deformation intensive region, such as the primary and secondary shear deformation zones, will be thereby resized to accurately reproduce such effects. Likewise, inactive areas will be coarsened, so computational resources are spared and better deployed [46].

3. Research Objectives and Methodology

3.1. Objectives

The goal of this study is to contribute to the existing knowledge on the machining of Ti-64 and Ti-555.3. To this end, a comparative study is conducted to outline the differences between these substantially distinct alloys from a machinability standpoint. A better understanding of machining conditions and mechanisms will set the foundation for upcoming optimization strategies. This document could also serve as a guide for selecting tooling and machining parameters for the turning of two titanium alloys.

3.1.1. Specific objectives

- Comparison of machinability related aspects of the titanium alloys: Ti-5Al-5V-5Mo-3Cr and Ti-6Al-4V.
 - o Developing a Finite Element (FE) model for wet turning of Ti-5Al-5V-5Mo-3Cr and Ti-6Al-4V.

- Running simulations for different cutting speeds, tool materials and coolant delivery strategies, such as flood and high-pressure coolant (HPC).
- Performing cutting tests for the selected conditions based on: temperature, cutting forces and stress data provided by the simulation.
- Collecting real-time data and performing post-process analysis of the collected chips and worn cutting tools (refer to methodology section for detailed information).

3.2. Methodology

Figure 5 presents a summary of all tests and analyses contained in this work, as well as the resources employed to perform them:

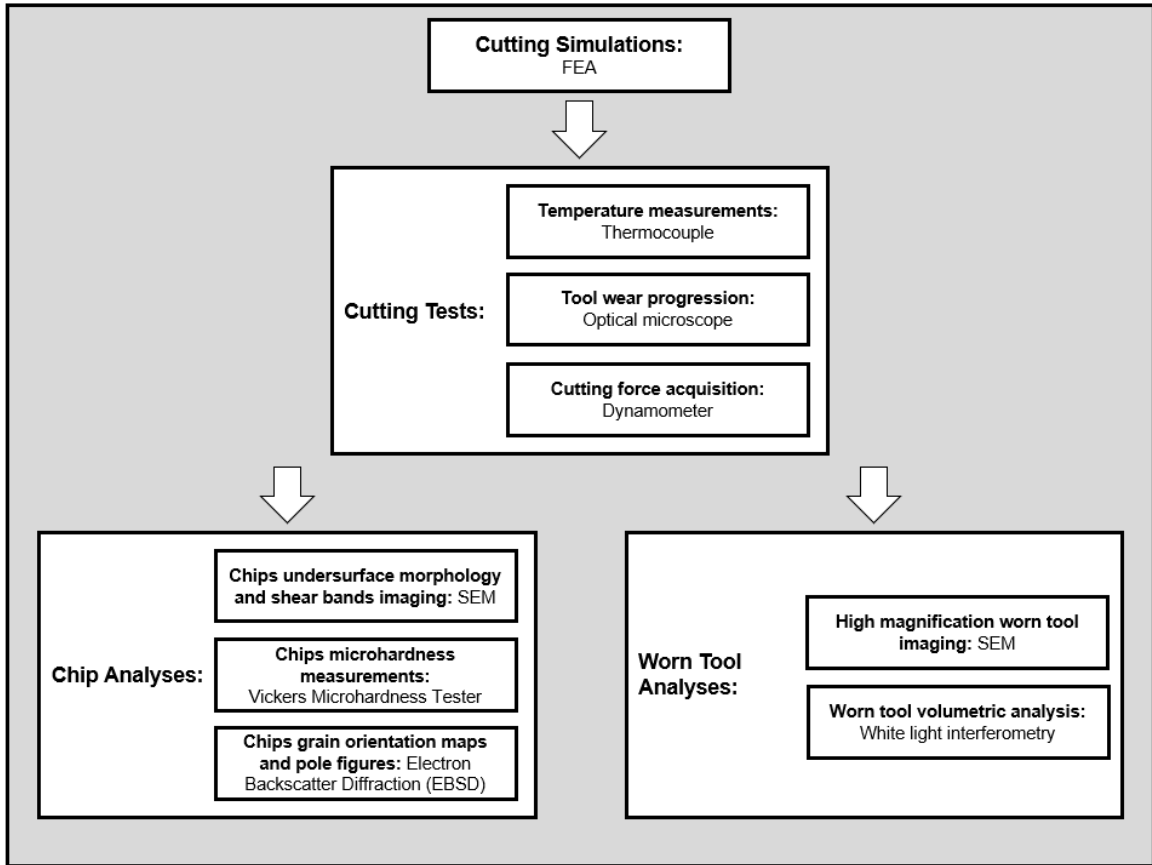


Figure 5: Experimental/FEA summary.

4. Materials and Methods

4.1. Finite Element Analysis (FEA)

The main purpose for the employment of FEA in this research is to obtain data that would not otherwise be readily available from experimentation, such as temperature and stress profiles. Additionally, allowing us to perform an extensive set of cutting tests without spending any resources on the acquisition of costly workpiece material and tooling.

In our case, the cutting tool was modeled as a rigid body where Coulomb's friction was applied to the relevant zones. All data inputs regarding simulation parameters were either obtained through a mesh convergence study or from the coolant supplier and are summarized in table 5.

Table 5: Simulation parameters for all the tested conditions.

Minimum element size (mm)	0.02
Maximum element size (mm)	0.1
Maximum number of nodes	24000
No. of output frames	30
Initial room temperature (°C)	20
Coolant heat transfer coefficient (W/m²K)	1x10 ⁴

In modelling the pressure effect of coolant, the velocity of the jet was inputted to the software. Which was calculated using the jet area based on the nozzle diameter, and the flow rate. It is assumed that the flow is uniform and steady after leaving the nozzle and that the speed of the jet is not appreciably reduced after hitting the chip. The pressure exerted by the jet is applied on the chip surface. The heat exchange between the chip and coolant was modeled as a convective thermal boundary condition. Orthogonal (2-dimensional) cutting was employed to simplify matters, as experimental validation attested to the validity of the model, implying a plain strain model does not account for the load distribution applied by the coolant in the Z axis. The simulated domain is displayed in figure 6.

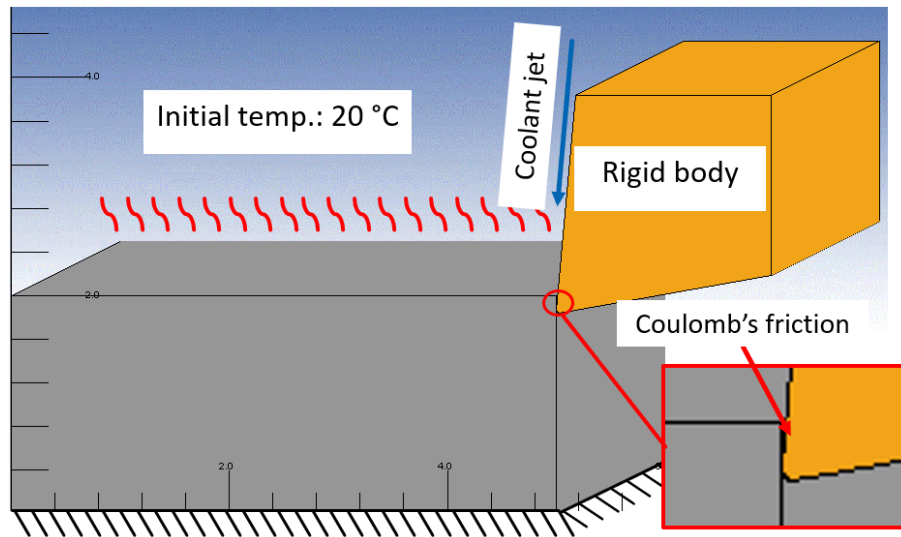


Figure 6: FEA model domain

A triangular mesh was employed, and all the constants were extracted from the software's pre-loaded material library, which contains a wide variety of aerospace alloys, along with other specialty and non-specialty materials.

Some of the materials' thermo-mechanical properties were listed previously in tables 2 and 4.

4.2. Experimental procedures

The cutting tests were performed on a SC-450 Nakamura-Tome CNC Lathe (figure 7a). The semi-synthetic, 6% concentrated, cutting fluid was supplied to the rake face of the commercially available Kennametal CNMG 432 uncoated Tungsten Carbide (WC) grade k turning insert by a ChipBLASTER J8-1000 High-

Pressure Coolant Supply, through Sandvik’s PCLNL 16 4DHP (figure 7b-c) Coolant-through tool holder.

ASTM B265 Grade 5 Ti-6Al-4V and Ti-5Al-5V-5Mo-3Cr workpieces (figure 7b), were used for all cutting operations. The workpieces were of a cylindrical shape measuring approximately 100 mm in diameter and 250 mm in length.

The selected cutting parameters are listed in table 6. The severe cutting conditions were selected to accelerate the wear rates and intensify the wear mechanisms on the uncoated cemented carbide tools as well as increase productivity levels (higher MMR), which is a factor of major interest to industry. This enables better visualization of the cutting process phenomena as well as highlights the role played by the HPC supply.

Table 6: Machining parameters for experimental testing.

	Coolant pressure (psi)				Feed (mm/rev.)	DOC (mm)
	Flood (Benchmark)	400	800	1000		
Vc (m/min)	150				0.1225	0.25
	n/a	200				
	n/a	250				

Based on the results obtained for Ti-555.3, an extra set of cutting conditions was introduced for the simulations and experiments. As tool life results were below expectations and the proposed cutting speeds were not suitable for the visualization of some wear and chip formation phenomena. Therefore, a lower

cutting speed of 40 m/min and the highest coolant pressure of 1000 psi were included in the conditions listed in table 6.

Cutting forces during the first 50 meters of cutting were measured by a three component Kistler 9121 tool holder dynamometer (figure 7b) transmitted to a Kistler 5010 amplifier and recorded using LABVIEW 14.0.

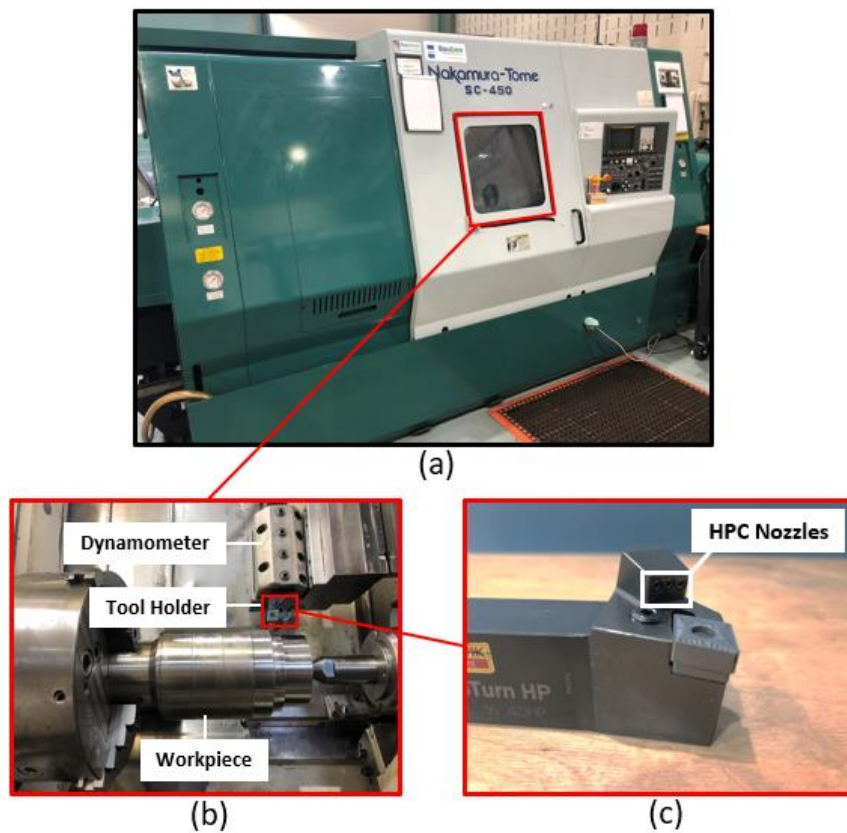


Figure 7: (a) Machine tool, (b) workpiece, dynamometer, tool holder setup and (c) detailed view of tool and coolant-through tool holder.

As shown in figure 8, a thermocouple was positioned close to the rake face of the cutting tool. The insertion was made by Electrical Discharge Machining (EDM) to enable acquisition of peak temperature measurements [24], [47], [48]. This setup was performed exclusively for modeling validation. Unaltered cutting tools were employed in the actual cutting tests.

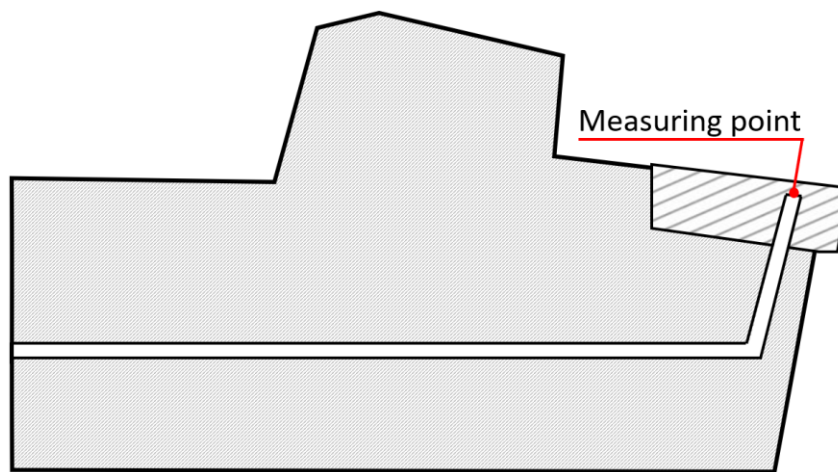


Figure 8: Experimental temperature measurement point.

Chips were collected at the end of the first cutting step so that the tool/chip contact conditions would not be affected by the geometry changes caused by tool wear. The maximum flank wear criterion was set to 300 microns (according to ISO 3685) or 2500 meters of cutting length, whichever occurred first. Flank wear measurements were taken at increments of 100-150-meters. Optical microscopy images (KEYENCE VHX-5000) of the worn inserts' rake and flank surfaces were collected. A Tescan VEGA2 Scanning Electron Microscope (SEM) was used to

acquire high magnification images of chip surface topography and worn cutting inserts to assess the tool/chip contact behavior during the machining process. Additionally, orientation maps were obtained by Electron Backscattered Diffraction (EBSD) using a JEOL JSM-7000F Scanning Electron Microscope. Moreover, white light interferometry was carried out with an Alicona Infinite Focus optical microscope for 3D surface measurements of the worn inserts and collected chips. A high-resolution Nikon Eclipse LV100 optical microscope was used for the microstructural analysis of the chips' cross sections. Prior to imaging, samples were cold mounted, polished and etched by being swabbed with a cotton ball rinsed in a solution of HF + HNO₃ for 10 seconds.

Microhardness measurements of the collected chips were performed by a Matsuzawa MMT-X7A micro Vickers hardness tester with a diamond quadrangular pyramid indenter at 50 gf for 10 seconds.

5. Results and Discussion: Ti-6Al-4V

5.1. Finite Element Analysis (FEA)

As can be seen in figure 9, the simulation results feature slightly higher temperature values compared to the experimental data but the trend remained the same. This difference in temperature could be attributed the thermo couple being positioned a few millimetres away from the tool-chip interface [24], [48] (figure 8). In addition, a slight decrease in peak temperature was observed when comparing both conditions at 150 m/min (figure 9 a,b). This can be attributed to the reduced contact pressure and consequently elevated friction conditions generated by the HPC jet. While the overall temperature changes are not so significant, figure 9 (d-f) reveals a considerable difference in the peak temperatures of the chips. This result indicates that a higher amount of heat is being directed from the rake face into the chip, which is a highly desirable outcome when machining difficult-to-cut alloys. Excess heat at the rake face of the cutting tool facilitates the diffusion process, which accelerates crater wear and reduces tool life. As crater wear

progresses, material is being removed from the insert, thus weakening the tool's cutting edge, ultimately leading to its catastrophic failure.

As shown in figure 9 (e, f), the additional momentum provided by the HPC jet creates some regions of concentrated strain, where chips are most susceptible to breaking. However, the same cannot be said for the flood condition presented in figure 9-d, where the chip curls to its natural unobstructed radius. This indicates a continuous chip formation that might lead to poor surface finish, excessive heat accumulation and ultimately, premature tool failure.

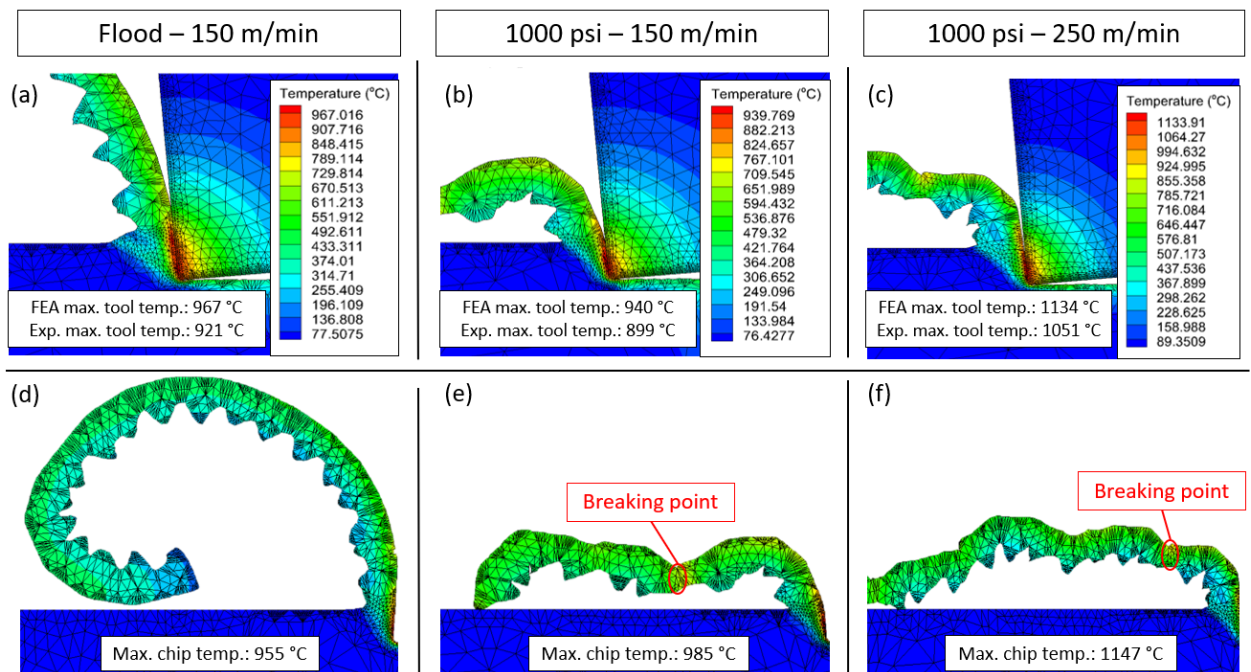


Figure 9: Temperature measurements for both simulation and experimental conditions of Ti-6Al-4V combined with FEA results for chip formation at (a,d) flood – 150 m/min, (b,e) 1000 psi – 150 m/min and (c,f) 1000 psi – 250 m/min.

A notable reduction in TCCL for the two HPC scenarios is presented in figure 10. The changes were about 50% for the 150 m/min (figure 10-b) and 250 m/min (figure 10-c) HPC conditions. The minimum stress concentration is directly correlated with the length of the contact region and is partially responsible for the diffusion and adhesion wear mechanisms. Additionally, a reduction in contact pressure is visible for the two HPC scenarios (figure 10), indicating a less intensive overall stress profile. High contact loads are some of the main facilitators of the adhesion process, once the adhesive bond's strength is proportional to the pressure being applied. The eventual tear off of the welded workpiece material will cause what is known as plucking, causing damage similar to the diffusion process.

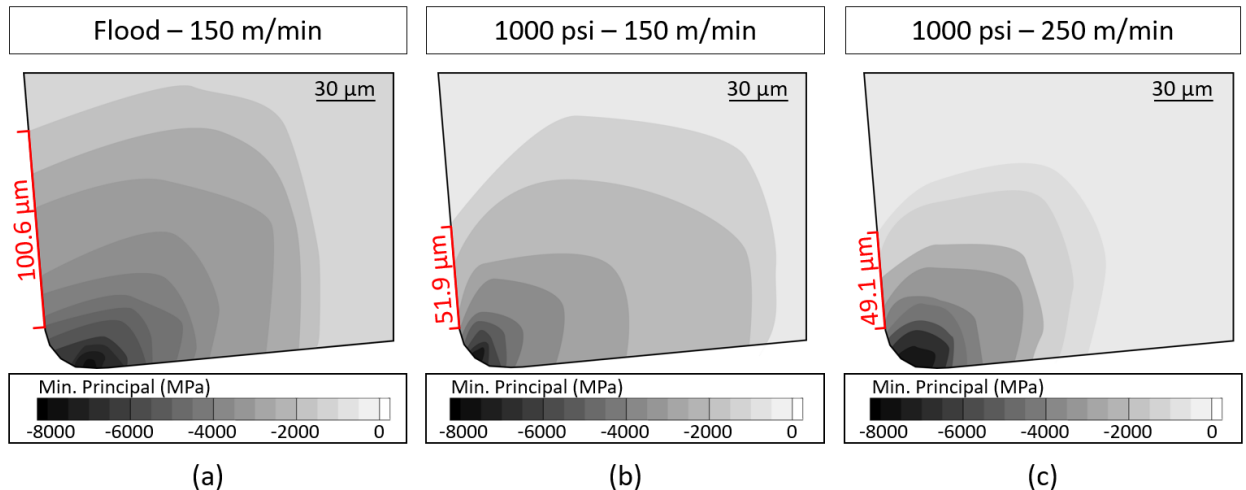


Figure 10: Tool stress profiles and TCCL for Ti-6Al-4V at (a) flood – 150 m/min, (b) 1000 psi – 150 m/min and (c) 1000 psi – 250 m/min.

5.2. Tool Life

Figure 11 presents experimental data providing a direct tool life comparison between all the tested conditions. The graph shows the maximum flank wear at the same cutting length (as displayed on the graph) for each set of cutting parameters proposed in table 6. The length is determined by the point of failure (when flank wear exceeds the pre-established end of life criteria) for the worst performing coolant pressure at a specific cutting speed.

A trend can be noticed in figure 11, with regards to maximum flank wear versus coolant pressure. Higher coolant pressures have a positive impact on wear rates throughout the cutting process due to the modified thermal and mechanical loads acting on the tool, as seen earlier in figures 9 and 10. Hoier et al. [49] highlighted similar behavior when machining Inconel 718. Cobalt binder present in the carbide insert's structure is subject to thermal softening, which facilitates its removal by abrasion. The temperature profiles shown in figure 9 support this conclusion. In the flood condition, heat is dissipated into the cutting tool instead of being expelled by the chips. Furthermore, this also accounts for the higher flank wear rates measured at cutting speeds of 200 m/min and 250 m/min.

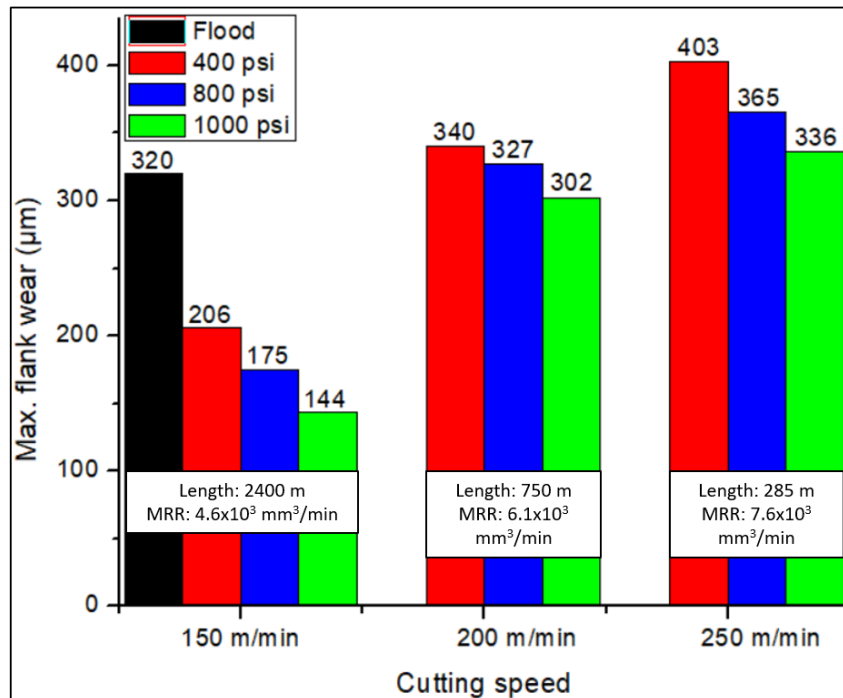


Figure 11: Flank wear comparison chart + MRR values for all conditions of Ti-6Al-4V.

As shown in figure 12, when cutting at the lowest speed of 150 m/min with HPC, inserts reached 2500 meters of cutting length without meeting the pre-established end of life criteria (flank wear of 300 µm). In fact, when looking at the wear curves in figure 12, flank wear was less than half of that of the flood benchmark condition. Similar results were obtained at the highest cutting speed of 250 m/min, where the best tool life was observed at the same pressure of 1000 psi.

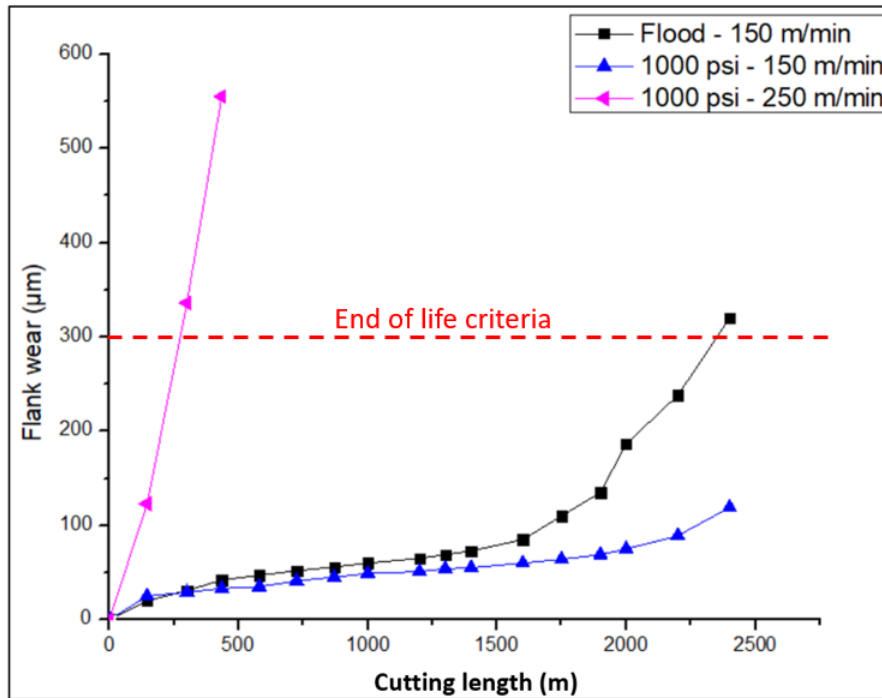


Figure 12: Tool wear progression curves for Ti-6Al-4V at flood – 150 m/min, 1000 psi – 150 m/min and 1000 psi – 250 m/min.

After three measurements, cutting forces (figure 13) were also significantly lower for the HPC compared to the benchmark, which is in accordance with the data obtained from simulation. A cutting force reduction of 40% at 150 m/min can be attributed to the more efficient chip evacuation, requiring less power from the machine tool to produce the cut. A correlation can also be established between the stress profiles seen in figure 10 and the cutting forces in figure 13, once the compressive loads that act against the cutting movement are clearly greater in the flood condition. Cutting forces are thus mainly dependant on the area of the shear

planes [24], [29]. The reduction in TCCL has a direct impact on the values observed in the two HPC conditions. These results are in agreement with previous research performed by Jagtap et al. [50]. As a consequence, further analyses were narrowed down to the benchmark flood condition and the following two sets of parameters: 150 m/min at 1000 psi and 250 m/min at 1000 psi to highlight the factors leading to the notable improvement in tool wear and cutting forces.

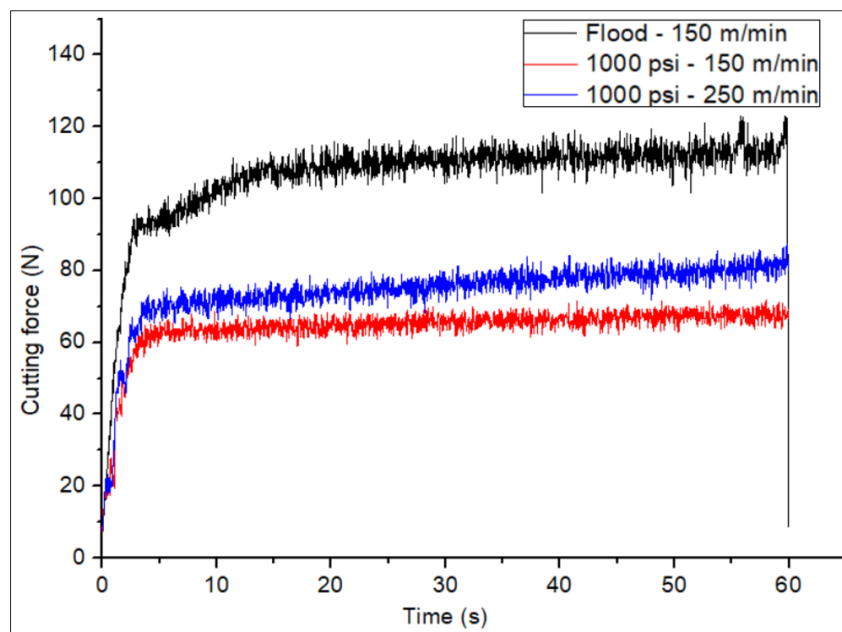


Figure 13: Cutting forces for Ti-6Al-4V at flood – 150 m/min, 1000 psi – 150 m/min and 1000 psi – 250 m/min.

For matters of validation, cutting forces were compared to those obtained by FEA. Simulated forces remained within a 10% margin from the experimental results for both materials. Figure 14 is an example of such results.

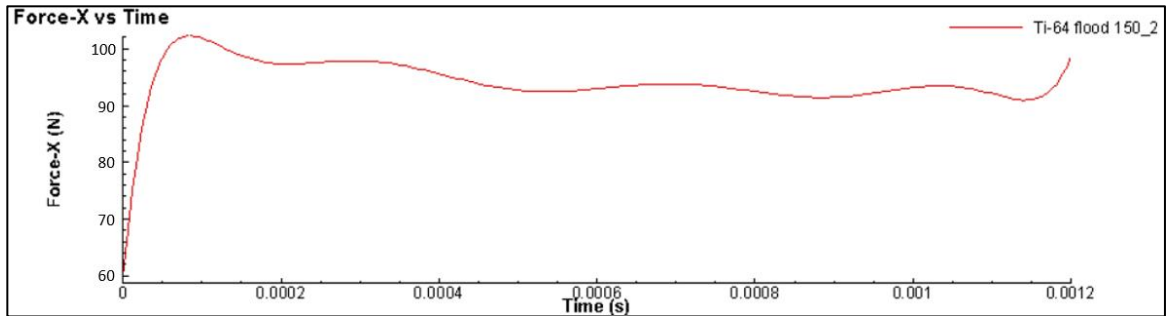


Figure 14: FEA cutting forces for flood – 150 m/min

5.3. Tool Wear Modes and Mechanisms

Secondary Electron (SE) SEM images were taken from the worn tools' rake and flank faces to identify the main wear modes during the cutting process. In figure 15 (a-c), the predominance of adhesion and diffusion over other wear mechanisms becomes evident, which cause the formation of Built-up edge (BUE) and crater wear modes. These images also show a positive influence of cutting speed on the BUE formation [24], [29], [51]. In figure 15-a, the crater wear is about twice as intense as the crater wear at the same cutting speed when HPC is used (figure 15-b), indicating a shorter contact length at the HPC condition. The presence of oxidation wear is only noticeable in the flood condition (figure 15-a). Oxidation is normally found near the end of the contact region, as a result of the reaction between oxygen and the tool binder [24]. Less intense sliding contact pressure in this area promotes oxygen flow and the ensuing oxidation reaction. Furthermore,

abrasion marks were more pronounced at the high-speed conditions in figure 15-c, lowering the tool life. Abrasion is visible since there is not a substantial volume of material adhered to the flank face of the insert.

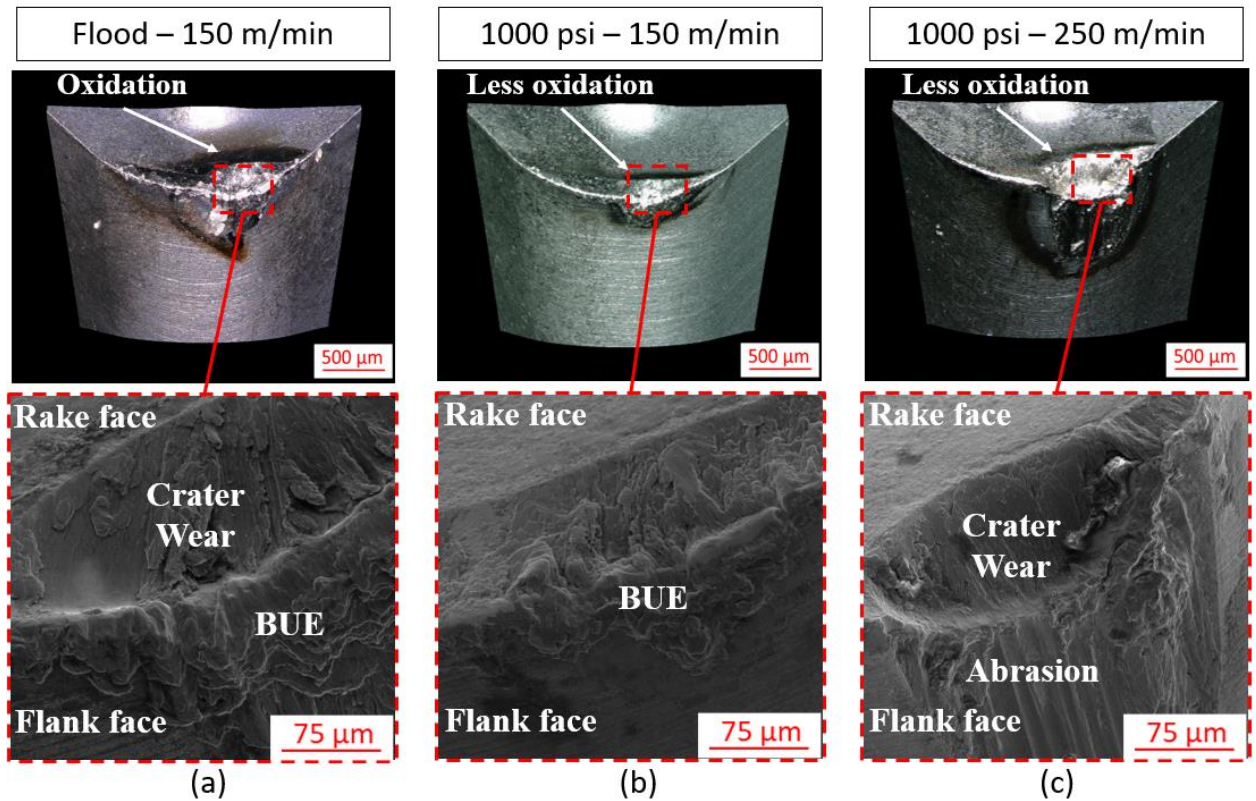


Figure 15: SEM of worn inserts for Ti-6Al-4V at (a) flood – 150 m/min, (b) 1000 psi – 150 m/min and (c) 1000 psi – 250 m/min, indicating the presence of oxidation, crater, BUE and flank wear modes.

Further volumetric analysis showed that in both HPC scenarios, the amount of adhered material represented by V_p (Volume of peaks above reference), is in fact less than that of the flood condition (Figure 16 b,c). Less adhesion can be

observed at a higher cutting speed (figure 16-c). However, V_v (Volume of valleys below reference), or the volume of removed tool material, is noticeably higher at this speed. This number is not only related to crater wear, but also the highly pronounced abrasion at 250 m/min due to the softening of the tool binder.

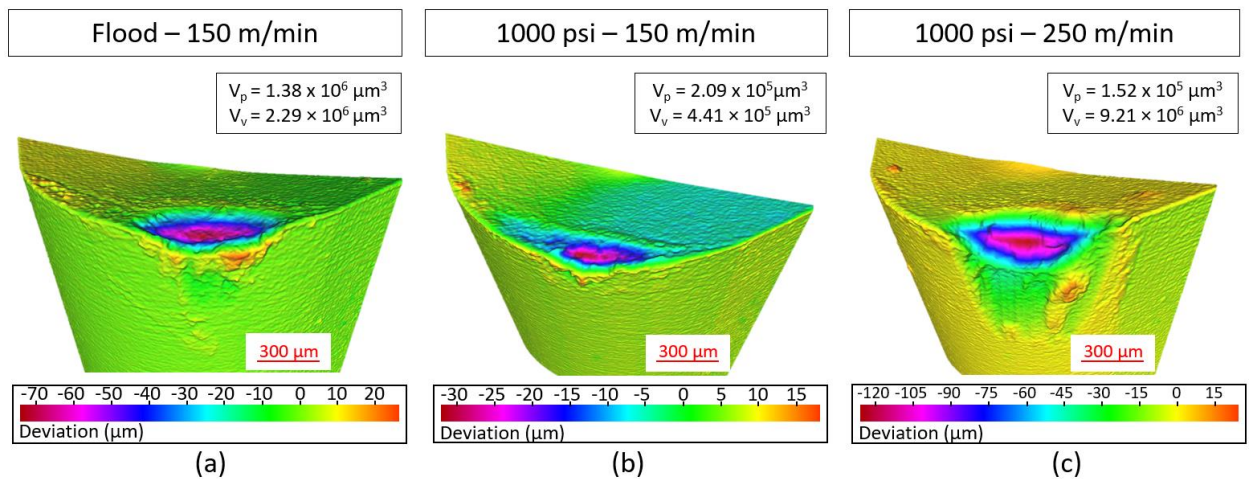


Figure 16: Volumetric analysis of worn tools for Ti-6Al-4V at (a) flood – 150 m/min, (b) 1000 psi – 150 m/min and (c) 1000 psi – 250 m/min, indicating the volumes of adhered and removed material from the cutting inserts.

There are three main contributors to the featured wear mechanisms: contact, load and chemical affinity. HPC promotes the separation between the chip and the rake face of the cutting tool, thereby reducing the contact length as well as the mechanical loads acting on that region, which can be supported by the simulation results in figures 9 and 10.

5.4. Chip Analysis

Secondary electron images of the chips undersurface and shear bands were taken to evaluate the influence of HPC on chip morphology. Some inclusions were more frequent on the undersurface of the studied chips (figure 17-a) under the HPC condition. This can be due to the sticky nature of contact for those conditions. To confirm this hypothesis a longer sliding contact region was detected in the benchmark flood scenario (refer to figure 15).

Images shown in figure 17-b reveal that segmentation is present in all of three tested conditions. In general, segmented chips are common when machining alloys with high hardness and low thermal conductivity, such as titanium [52]. In some situations, segmented chips may be desirable for cutting force reduction and enhanced chip evacuation [53]. Furthermore, the segmentation edges are smoother when working with a high-pressure coolant supply. The shear band formation process is facilitated by the application of HPC, which may account for the force reduction in figure 13. As stated by Dargusch et al. [52], tool wear will also affect the chip formation process as well as the segmentation and deformation of chips throughout the course of machining.

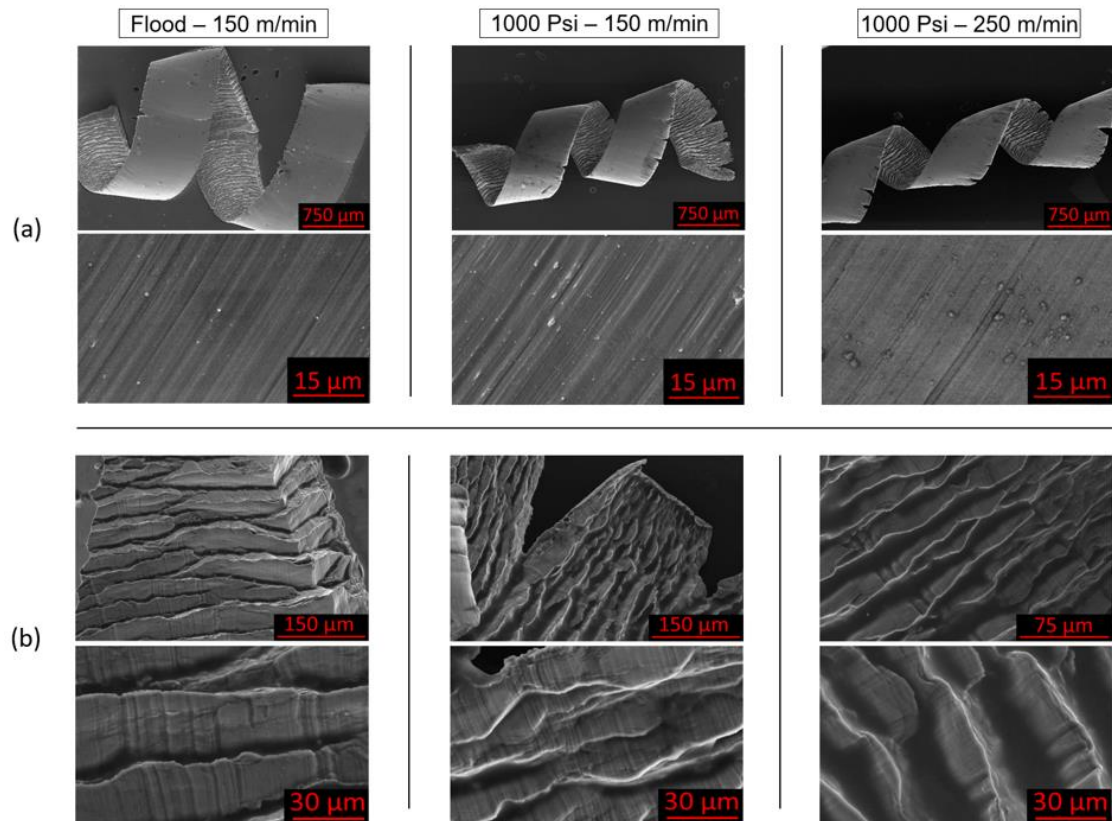


Figure 17: SEM of (a) chip undersurfaces and (b) shear bands for Ti-6Al-4V.

Based on the experimental results of chip formation and tool wear mechanisms, the schematic diagram in figure 18 illustrates the changes at the tool/chip contact area when applying HPC. In figure 18-a, the normal stress decreases exponentially along the contact region and is inversely proportional to the chip sliding velocity, becoming maximum at the tool tip and minimum at the point where chip loses contact with the cutting tool. The normal stress and sliding velocity profiles contribute to the definition of the sticking and sliding regions. The

first one being characterized by high levels of contact pressure and significantly low chip sliding velocity, and the second one where pressure is reduced, enabling the chip to flow at a higher speed. These contact conditions change once HPC is introduced. As presented in figure 18-b, HPC reduces the contact pressure (normal stress) to a certain level, where the chip immediately loses contact with the tool's rake face, preventing the sliding interaction. On this basis, a direct correlation can be drawn from the tools analyzed in figure 15, where oxidation was not intense under the HPC conditions. This indicates a substantially shorter low pressure contact area. The chips in figure 17, with inclusions on the collected samples, also characterize a process of a “sticky nature”.

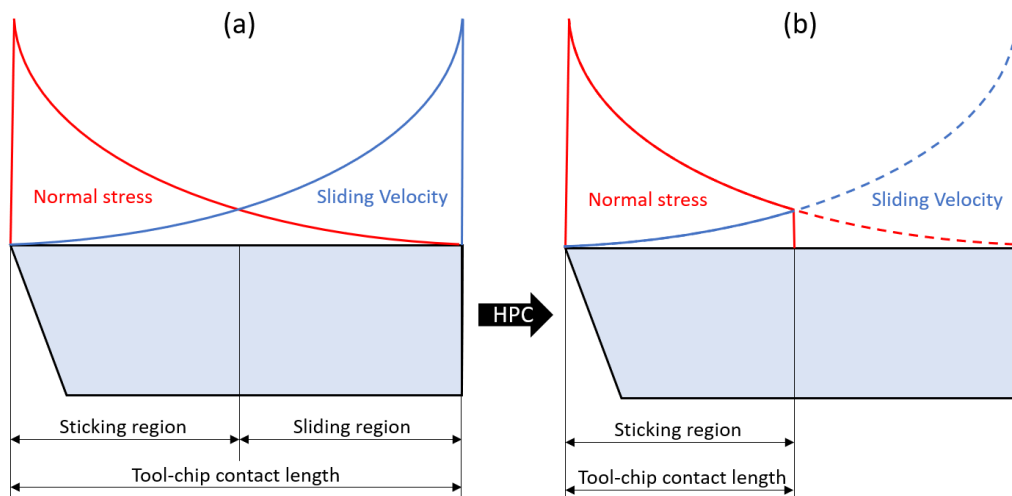


Figure 18: Tribological conditions along the rake face of the insert for Ti-6Al-4V at (a) dry / flood, and (b) high-pressure coolant conditions.

To investigate the role of HPC as well as the cutting speeds on the shear bands, the chip cross sections were analyzed with EBSD, with the results presented in Figure 19. The orientation maps of the regions taken from the chips in Figure 19 (a, c, e) are shown in Figure 19 (b, d, f), respectively. It can be observed that the grains are more elongated at higher cutting speeds (Figure 19-f) compared to lower cutting speeds (Figure 19-d). The same can be stated when comparing HPC to flood conditions, due to the severe plastic deformation caused by HPC application. In this case, shear bands formed by flood coolant (Figure 19-b) have equiaxed grains ($\sim 1 \mu\text{m}$) compared to a mixture of equiaxed ($\sim 7 \mu\text{m}$) and highly elongated grains in HPC machining (Figure 19 (d, f)).

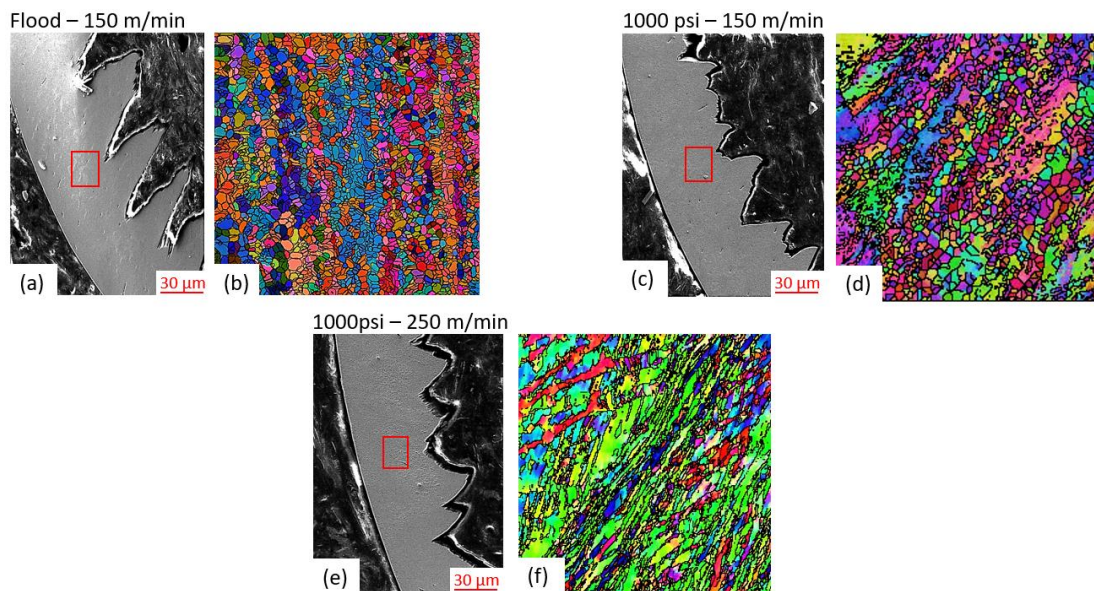
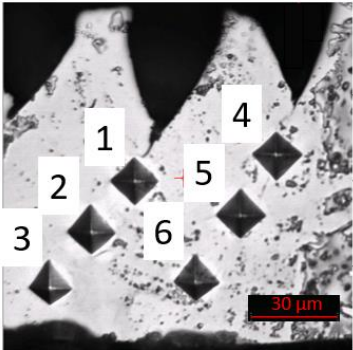


Figure 19: Chips cross-sections and EBSD orientation maps for Ti-6Al-4V at (a,b) flood – 150 m/min, (c,d) 1000 psi – 150 m/min and (e,f) 1000 psi – 250 m/min.

The micro hardness profiles in table 7 and figure 20 are in agreement with the EBSD data presented in figure 19, confirming that strain hardening results from the high deformation levels caused by the application of HPC. This becomes more evident for the areas close to the tool-chip contact region, where the variation in hardness is noticeably higher.

Table 7: Chips shear bands microhardness profiles for Ti-6Al-4V at flood – 150 m/min, 1000 psi – 150 m/min and 1000 psi – 250 m/min with values highlighted for the points located near the tool-chip interface.

	Hardness (HV)					
	1	2	3	4	5	6
						
Flood – 150 m/min	337	365	361	306	330	354
1000 psi – 150 m/min	354	365	392	354	396	380
1000 psi – 250 m/min	373	363	434	343	338	408

* All values are subject to a variation of $\pm 5\%$

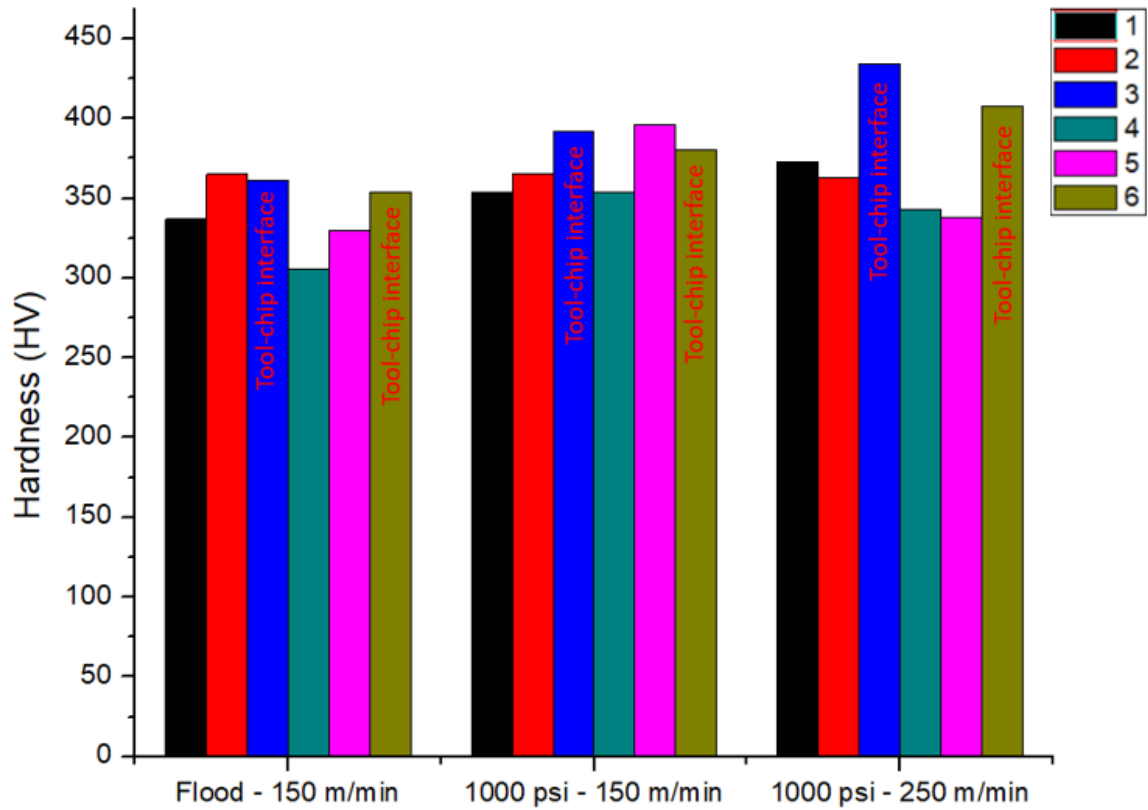


Figure 20: Chips shear bands microhardness values for Ti-6Al-4V at flood – 150 m/min, 1000 psi – 150 m/min and 1000 psi – 250 m/min with the points located near the tool-chip interface highlighted.

The severe plastic deformation imposed by HPC causes the chips to strain harden. Once they become more fragile, their breakability is improved.

6. Results and Discussion: Ti-5Al-5V-5Mo-3Cr

6.1. Finite Element Analysis (FEA)

Comparing figure 21 to figure 9, tool and chip peak temperatures are approximately 30% lower when comparing Ti-555.3 to Ti-64 at the same machining conditions. Although these results contradict this material's lower thermal conductivity [20], [54], [55] (table **Error! Reference source not found.**), they reflect its longer TCCL (see figure 22) and consequently reduced peak contact stresses at the Secondary Shear Deformation Zone (SSDZ) (figure 22). Therefore, heat is distributed over a larger area on the rake face of the cutting tool.

The variation in tool peak temperature is insignificant among the simulated cutting conditions. These results agree with the small variation in TCCL presented in figure 22, since the coolant is still unable to access the exact area of peak heat generation.

The positive effect of HPC on chip control becomes evident when analyzing figure 21 (d,g,h), where a considerable reduction in chip curl radius can be seen, which is comparable to that found in the experiments, except at low speeds (figure

21-d). HPC deliver's pressure to the chip's undersurface, increasing the amount of strain and improving its breakability. This same phenomenon was observed in Ti-64 (figure 9) and is considered to be one of the main benefits provided by the application of HPC [12].

As can be seen in figure 21 (c,d,g,h), peak chip temperatures were recorded at the points of higher plastic deformation, usually located near the chip breaking points.

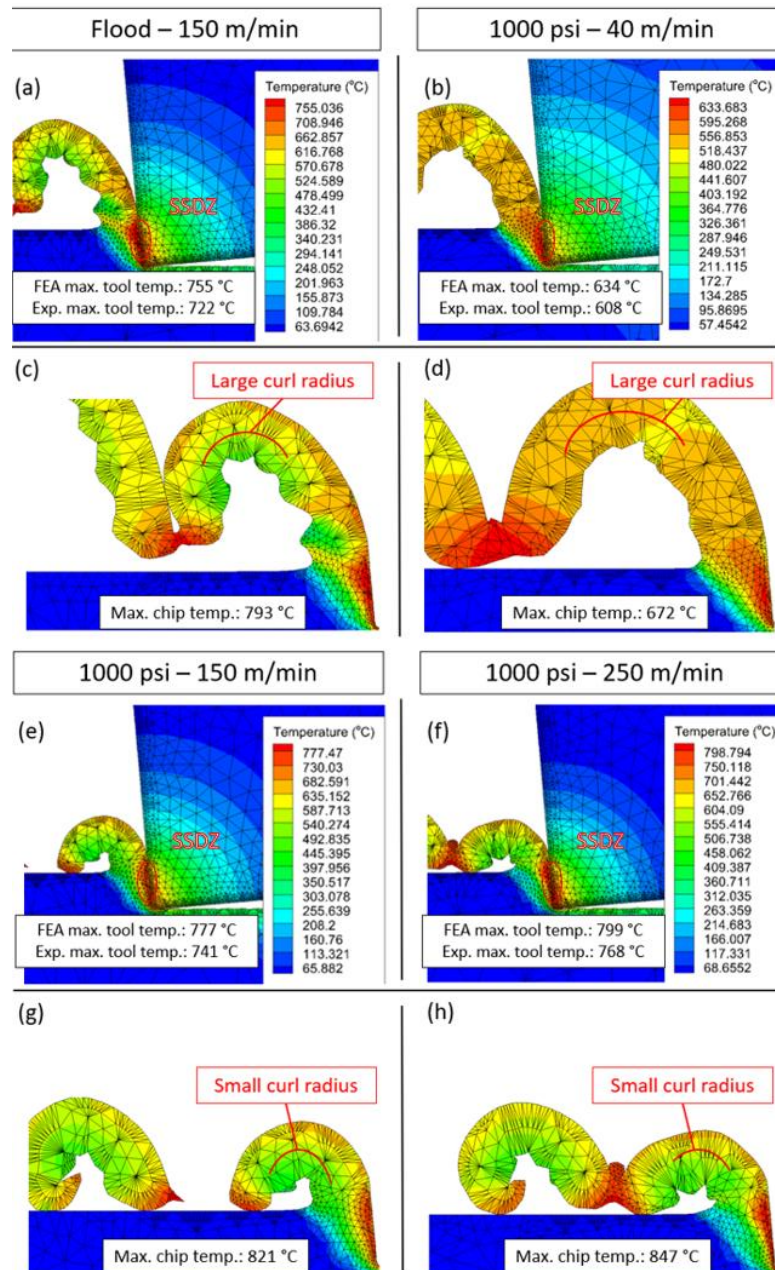


Figure 21: Temperature measurements for both simulation and experimental conditions of Ti-5Al-5V-5Mo-3Cr combined with FEA results for chip formation at (a,c) flood – 150 m/min, (b,d) 1000 psi – 40 m/min, (e,g) 1000 psi – 150 m/min and and (f,h) 1000 psi – 250 m/min.

A short TCCL and highly concentrated compressive stresses are common features of titanium alloy machining [22]. However, in the Ti-555.3 simulations, TCCL remained relatively high and presented little to no variation throughout all of the cutting conditions, in contrast with what was observed for Ti-64 (figure 10). Therefore, no visible difference in the general stress profiles could be noticed when comparing flood and HPC scenarios at the same cutting speed of 150 m/min (figure 22 a,c). Furthermore, a notable reduction in peak compressive stresses is only visible when reducing the cutting speed to 40 m/min. As a result, the wear phenomena taking place on the rake face of the cutting tools, such as diffusion and adhesion between tool and workpiece material, should not be greatly affected by the application of HPC when working with Ti-555.3. Tool wear modes and mechanisms will be further investigated in the “Tool wear modes and mechanisms” section (figure 25).

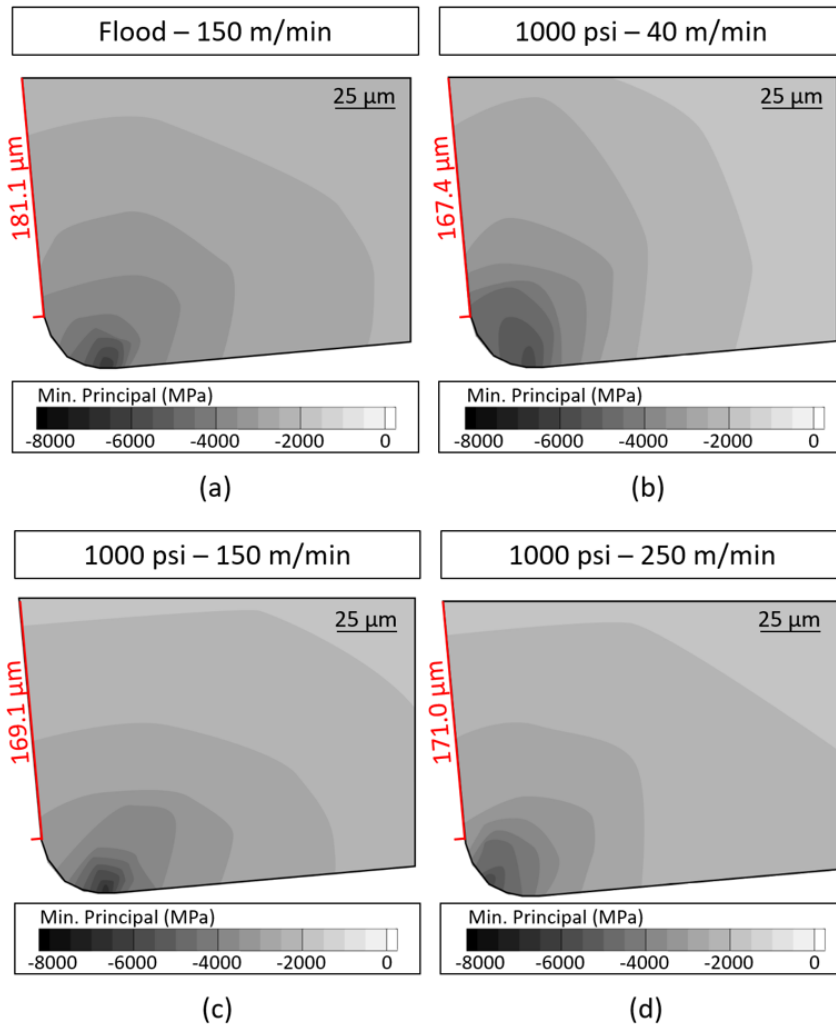


Figure 22: Tool stress profiles and TCCL for Ti-5Al-5V-5Mo-3Cr at (a) flood – 150 m/min, (b) 1000 psi – 40 m/min, (c) 1000 psi – 150 m/min and (d) 1000 psi – 150 m/min.

6.2. Tool Life

When machining Ti-555.3 inserts would reach the pre-established end of life criteria after less than 40 meters of total cutting length (figure 23). On that premise. Shorter passes were thus taken to obtain proper tool wear progression curves. (figure 23-b).

The worst tool life results were recorded for the benchmark flood condition and at the highest speed of 250 m/min and coolant pressure of 1000 psi (figure 23). Under these conditions, inserts were only able to reach about 20 meters of cutting length prior to exceeding 300 μm of flank wear. An approximate 30% improvement was observed for the other two sets of parameters.

The intensity of the measured flank wear in figure 23 indicates a substantial presence of hard particles in the material's structure [24], which significantly hinders its machinability when compared with other grades of titanium alloys. The results presented in figure 12 show that Ti-64 clearly has better machinability as the registered tool life of Ti-64 was about 100 times longer at the same sets of cutting conditions compared to the near- β alloy, contradicting what was previously reported in literature.

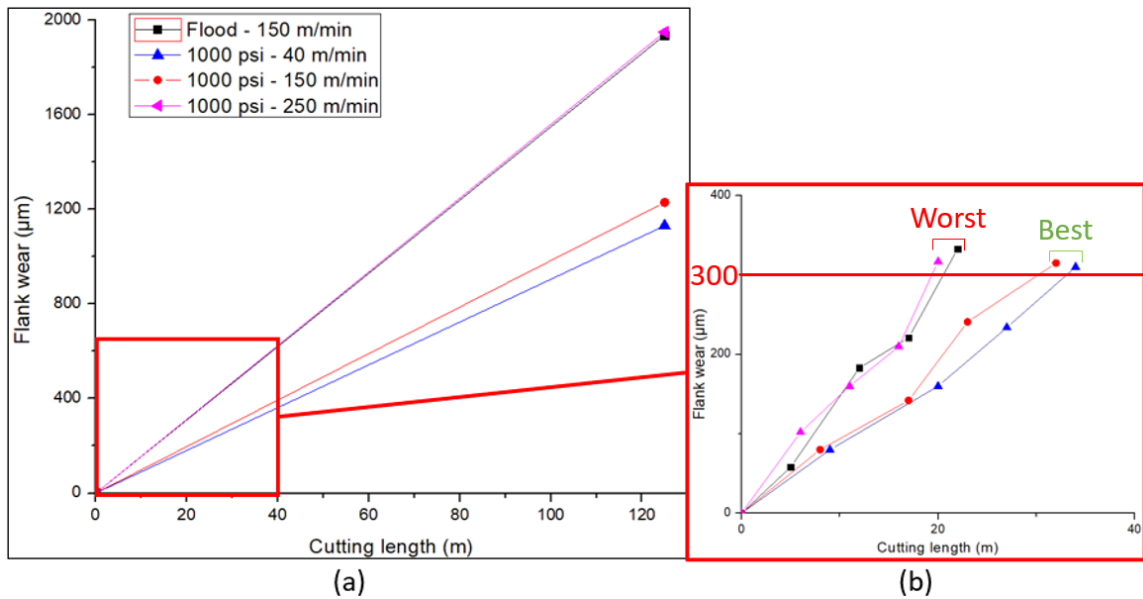


Figure 23: Tool wear progression curves for Ti-5Al-5V-5Mo-3Cr at flood – 150 m/min, 1000 psi – 40 m/min, 1000 psi – 150 m/min and 1000 psi – 250 m/min for (a) long and (b) short passes.

After three repetitions of the force measurements, cutting forces in figure 24, did not follow the same trend as the tool wear data curve (figure 23), as the highest values were actually obtained for the lower speed of 40 m/min. The highest values were actually obtained at a lower speed of 40 m/min. Results indicate an already expected inverse relationship between speed and cutting forces which was also true for the simulations, since at lower cutting speeds, the effects of thermal softening are not as significant as at the higher ones [24], [46], [56]. Nevertheless, results obtained at a speed of 150 m/min show that HPC reduces cutting forces, to an extent comparable to that reported in the previous chapter for the Ti-64 alloy

(figure 13). A slight drop is noticed during the cutting at 250 m/min which could also be an effect of thermal softening.

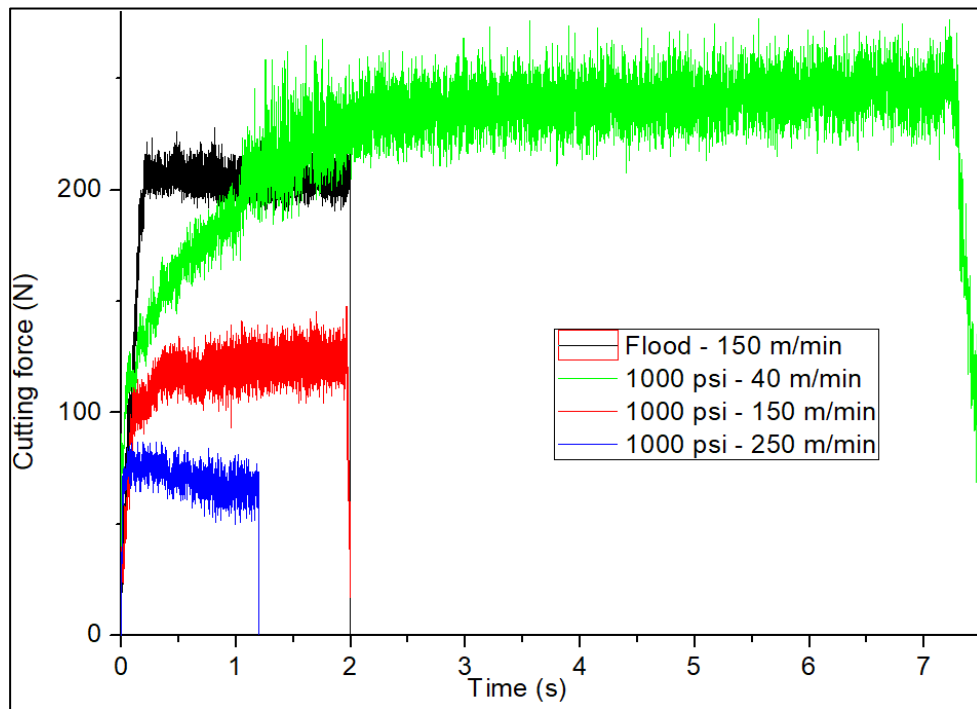


Figure 24: Cutting forces for Ti-5Al-5V-5Mo-3Cr at flood – 150 m/min, 1000 psi – 40 m/min, 1000 psi – 150 m/min and 1000 psi – 250 m/min.

6.3. Tool Wear Modes and Mechanisms

In figure 25, the dominance of abrasion and adhesion over other wear mechanisms becomes evident, leading to the formation of a Built-up edge (BUE) and intensive flank wear. Flank wear evolves at a much higher rate compared to Ti-64 under the same cutting conditions, indicating the presence of hard carbide

inclusions in the workpiece material. Even at the lowest cutting speed of 40 m/min in figure 25-b, the flank wear severity exceeds that of Ti-64 at the highest cutting speed of 250 m/min (figure 15-c).

As a consequence of cyclic plucking of adhered workpiece material from the tool's cutting edge, chipping is also visible in all the cutting conditions.

There is not a substantial amount of visible crater wear in figure 25. Therefore, these results agree with the temperature and stress gradients presented in figures 21 and 22, since the diffusion process relies on intensive heat generation and severe contact conditions at the tool-chip interface [24], [29].

The only visible effect from the application of HPC is the reduction in oxidation wear at the rake face of the cutting tools (figure 25 b,c,d), indicating a less intense sliding contact pressure near the end of the tool-chip contact length.

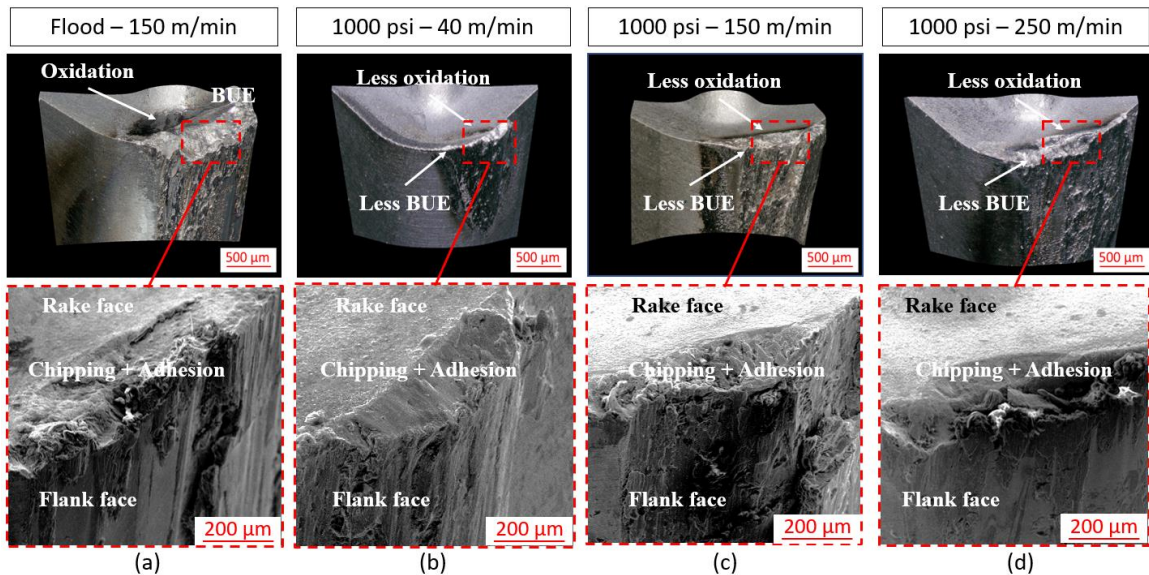


Figure 25: SEM of worn inserts of Ti-5Al-5V-5Mo-3Cr at (a) flood – 150 m/min, (b) 1000 psi – 40 m/min, (c) 1000 psi – 150 m/min and (d) 1000 psi – 250 m/min, indicating the presence of oxidation, edge chipping, BUE and flank wear modes.

Further volumetric analysis showed that in all the HPC test conditions the amount of adhered material and removed material, represented by Volume of peaks (V_p) above reference and Volume of valleys (V_v) below reference), are in fact reduced (figure 26 b,c,d) compared to the flood condition. This is analogous to the phenomenon observed during the machining of Ti-64 at these same conditions (figure 16).

A difference in wear patterns can be noticed when comparing the SEM images and the volumetric analysis data of the tools used to machine the two studied alloys. Rake wear dominates during the machining of Ti-64 (figures 15-16),

whereas in Ti-555.3 (figures 25-26) the flank surface is the area most affected by wear, which reduces with the application of HPC, but increases with the rise in cutting speed due to the softening of the tool binder.

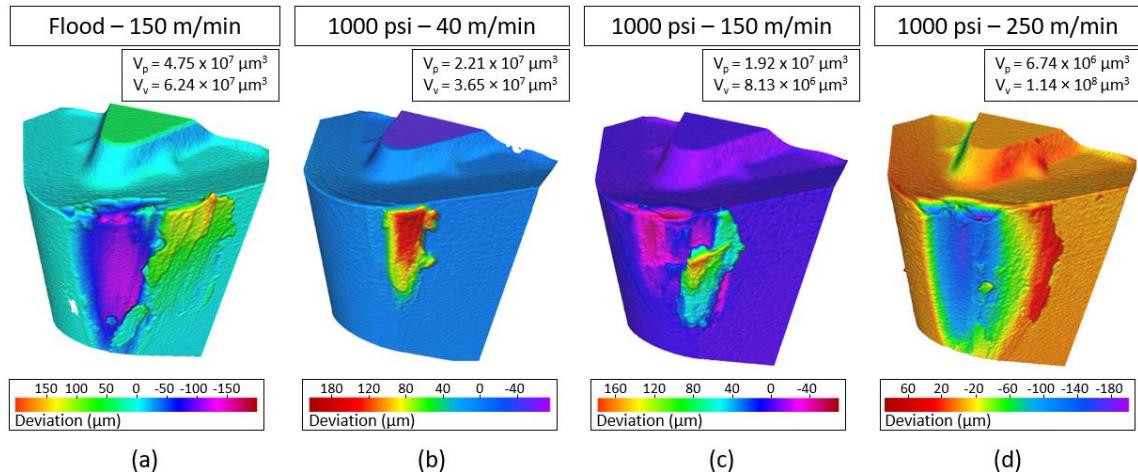


Figure 26: Volumetric analysis of worn tools for Ti-5Al-5V-5Mo-3Cr at (a) flood – 150 m/min, (b) 1000 psi – 40 m/min, (c) 1000 psi – 150 m/min and (d) 1000 psi – 250 m/min, indicating the volumes of adhered and removed material from the cutting inserts.

6.4. Chip Analysis

Secondary electron (SE) SEM images of the chip undersurface and shear bands were taken to compare the chip morphology of the two studied titanium alloys. At the lower magnification images in figure 27-a, the chip curl radius is considerably reduced (~50%) following the application of HPC. In addition,

changes in cutting speed also play a major role in chip control. Therefore, these results are consistent with the assumptions drawn from FEA data in figure 21.

Adhesive behavior was observed on the undersurface of the chips collected at 40 m/min (figure 27-a). This was attested by the presence of deep grooves and a significant amount of small imperfections distributed along the analysed area. These imperfections are results of the formation of adhesive bonds between the chips and the cutting tool [57], which allied to the cyclical plucking of adhered material which contributes to the tool edge chipping displayed in figure 25. At higher cutting speeds, the flow lines become more visible, denoting a smooth sliding process.

An inverse relationship between cutting speed and shear band frequency can be found in figure 27-b, comparable to that observed for Ti-64 (figure 17-b). Additionally, the distribution of shear bands along the horizontal length of the chip is not homogenous, which could be a consequence of the cutting depth variation provided by the tool nose radius, as reported by Wagner et al. [4]. Although, further investigation is necessary to confirm this hypothesis.

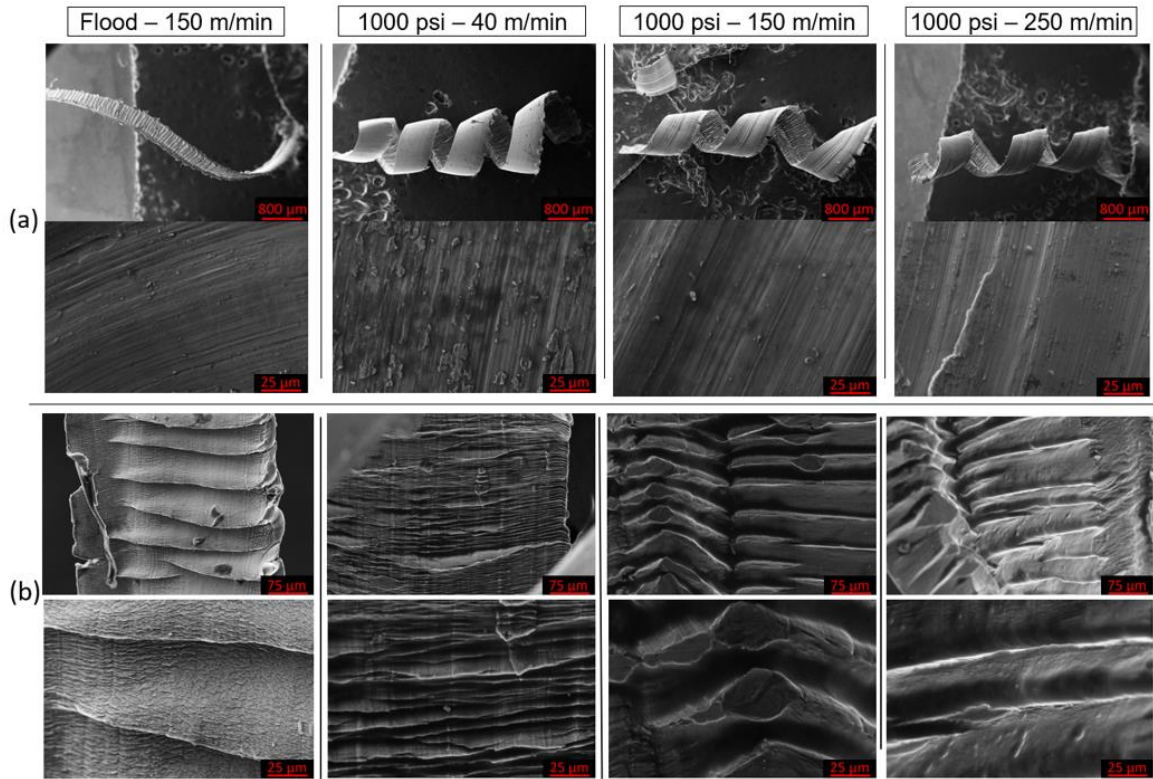


Figure 27: SEM of (a) chip undersurfaces and (b) shear bands for Ti-5Al-5V-5Mo-3Cr.

Based on the experimental results of chip formation and tool wear mechanisms, the schematic diagram in figure 28 illustrates the changes at the tool/chip contact area when applying HPC.

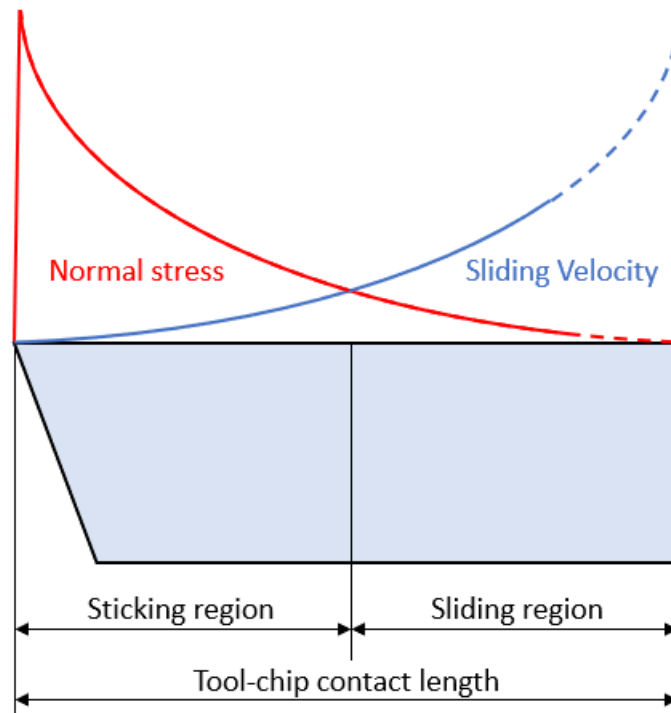


Figure 28: Tribological conditions along the rake face of the insert for Ti-5Al-5V-5Mo-3Cr at high-pressure coolant conditions.

To further investigate the role of HPC and conventional coolant systems as well as the cutting speeds on shear bands, the chip cross sections were analyzed using EBSD, with the data presented in figure 29.

Figure 29 (b-d) shows the EBSD contrast orientation maps at 40 m/m, 150 m/min, and 250 m/min, respectively for the same areas highlighted in figure 19 (a, c,e). Although some difficulty in the analysis arises from the presence of twins in the chips, the grains are visibly more elongated, especially when compared to the

chips obtained from conventional coolant (figure 29-a), confirming severe plastic deformation caused by HPC application.

The degrees of plastic deformation and heat generation are highly dominated by the cutting speed. Figure 29 (b-d) illustrates the orientation maps of the machined chips collected in different cutting speeds. It is noticed that the grains of chips collected at higher cutting speeds (150 m/min and 250 m/min, shown in figure 29 (c, d) are more deformed than those obtained at 40 m/min (figure 29-b).

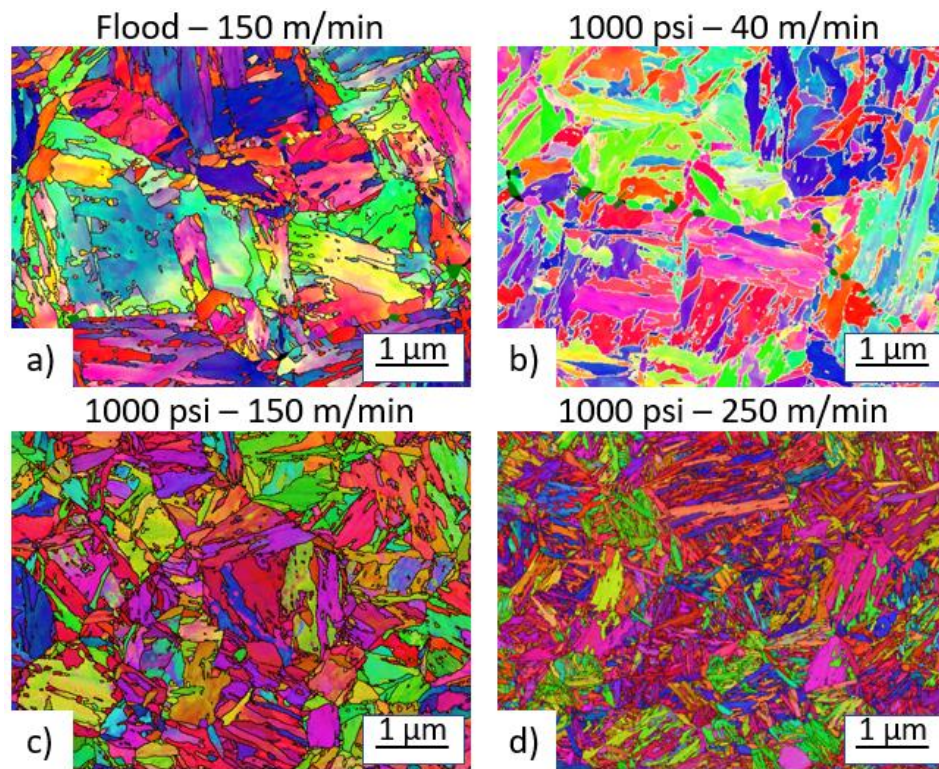
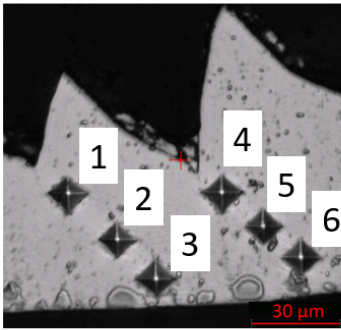


Figure 29: EBSD orientation maps for Ti-6Al-4V at (a) flood – 150 m/min, (b) 1000 psi – 40 m/min, (c) 1000 psi – 150 m/min and (d) 1000 psi – 150 m/min.

During Ti-64 machining, HPC induced deformation caused localized strain hardening to occur closer to the chip undersurface (table 7), However, in Ti-555.3, the highest hardness values were recorded at the center of the chips' cross-sections (points 2 and 5 of table 8 and figure 30), demonstrating that the coolant supply was unable to effectively permeate the tool-chip interface, thereby minimizing the role of strain hardening in that specific region. Therefore, the microhardness data presented in table 6 supports that the TCCL (figure 22) predicted by a model remains nearly unaltered at all cutting conditions. This phenomenon can be related to this material's elevated mechanical properties compared to Ti-64, which hinder the separation between tool and chip. In addition, stresses are more evenly distributed along the tool rake face compared to Ti-64.

Table 8: Chips shear bands microhardness profiles for Ti-5Al-5V-5Mo-3Cr at flood – 150 m/min, 1000 psi – 40 m/min, 1000 psi – 150 m/min and 1000 psi – 250 m/min with values highlighted for points located near the tool-chip interface.

	Hardness (HV)					
	1	2	3	4	5	6
						
Flood – 150 m/min	317	308	259	227	327	259
1000 psi – 40 m/min	312	347	341	290	369	312
1000 psi – 150 m/min	309	347	312	312	350	347
1000 psi – 250 m/min	337	350	330	309	340	324

* All values are subject to a variation of $\pm 5\%$

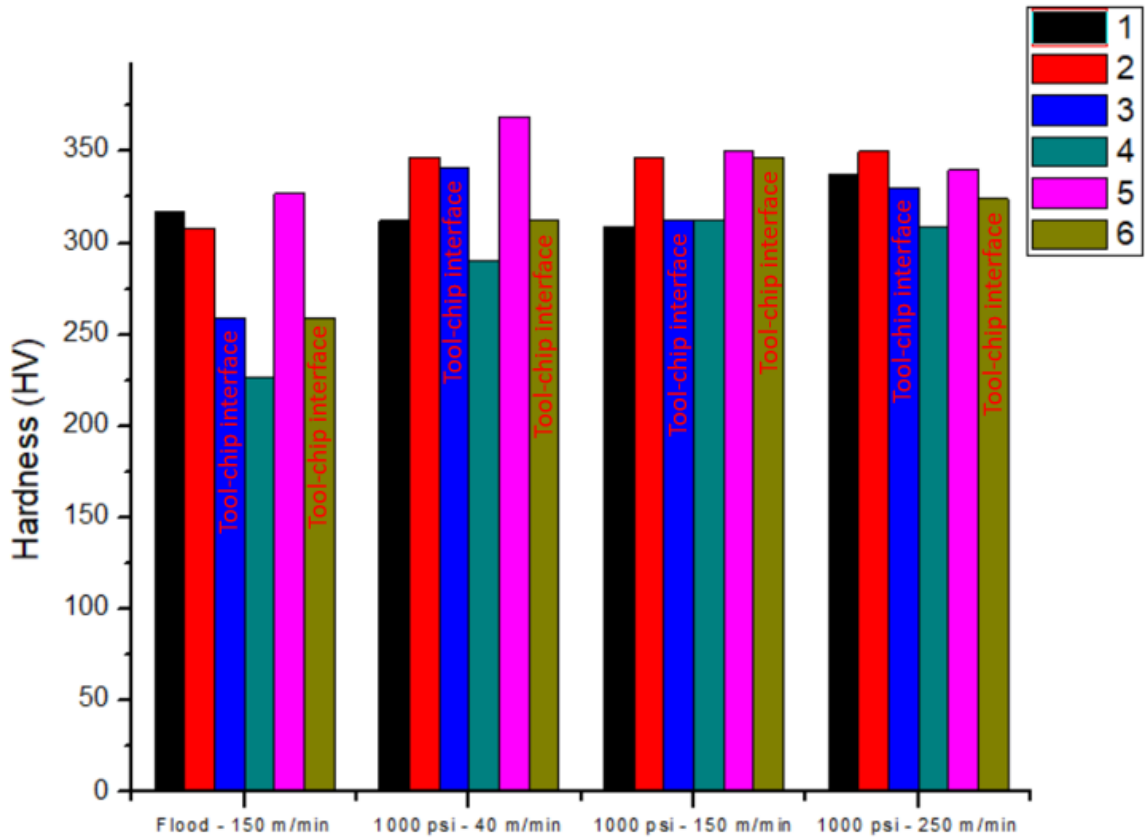


Figure 30: Microhardness values for Ti-5Al-5V-5Mo-3Cr at flood – 150 m/min, 1000 psi – 40m/min, 1000 psi – 150 m/min and 1000 psi – 250 m/min with points located near the tool-chip interface highlighted.

7. Conclusions

The research conducted in this study contributes to the existing knowledge on the machining of Ti-64 and Ti-555.3. A comparative study was carried out that outlines the differences between machining conditions, wear mechanisms and chip formation processes. Correlative relationships were established between coolant pressure, cutting speed, tool life, cutting forces, wear mechanisms and chip formation. Based on results obtained, the following contributions can be drawn.

1. Tool and chip peak temperatures are approximately 30% lower when comparing Ti-555.3 to Ti-64 at the same machining conditions. Although these results contradict this material's lower thermal conductivity, they reflect its longer Tool-Chip Contact Length (TCCL) and consequently reduced contact stresses in the Secondary Shear Deformation Zone (SSDZ), as seen in the stress profiles.
2. Modeling and experiments show a peak tool temperature reduction with HPC use during Ti-64 machining, which can be attributed to the reduced contact pressure and reduced friction conditions generated by the HPC jet. However, Ti-555.3 did not feature a considerable change in peak temperature at these same conditions, since the coolant was still unable

to access the exact area of peak heat generation, which can be attributed to this material's higher mechanical properties opposing the bending of the chip and thus avoiding its separation from the tool's rake face. Conversely, heat penetration into the cutting tool is considerably reduced by the application of HPC, demonstrating a general cooling effect.

3. The results presented indicate a clear superiority of Ti-64 in terms of machinability, since for the same set of cutting conditions, the registered tool life was about 100 times longer for this particular tool when compared to the Ti-555.3 near- β alloy. This difference is far larger than reported in the literature and is attributed to the tool used in this study.
4. When machining Ti-64, coolant pressure and maximum flank wear are inversely proportional to each other, indicating an influence of the heat directed towards the flank face of the cutting tool during the abrasion process. Although HPC reduces the flank wear rate in Ti-555.3, the possible presence of hard carbide inclusions in the material considerably reduces the tool life span. Other tool material choices with superior mechanical properties such as PCD and CBN coated tools, aiming for reduction in abrasion and chipping wear mechanisms, must be explored

in combination with higher coolant pressures to achieve optimal machining of near- β titanium alloys (Ti-555.3).

5. Oxidation wear is noticeably less intensive when HPC is used in the machining of both materials, suggesting less severe sliding interactions at the end of the tool-chip contact length.
6. Tool wear patterns differ greatly between both materials. Although there is a clear dominance of adhesion and diffusion over other wear mechanisms during Ti-64 machining, the flank wear develops at a much higher rate in Ti-555.3, causing the tool to prematurely reach its end of life criteria even when machining at a lower cutting speed. This phenomenon can be attributed to the material's higher mechanical properties and the presence of hard inclusions in its structure. However, this matter still requires further investigation.
7. As a consequence of the cyclic plucking of adhered workpiece material, severe chipping of the tool cutting edge was observed at all cutting conditions when machining Ti-555.3.
8. At higher cutting speeds, the presence of small imperfections along the chip's undersurface denotes a sticking process during Ti-64 machining,

whereas while machining Ti-555.3, the flow lines are more visible, indicating a smooth sliding process.

9. Previously described as a well-known outcome of Ti-64 machining, chip segmentation caused by the formation of adiabatic shear bands was also present in Ti-555.3, with its frequency being inversely proportional to the cutting speed.
10. In both cases, chip control is facilitated by the application of HPC, resulting in improved chip evacuation combined with a considerable reduction in the chip curl radius. This is attributed to the additional bending moment being applied to the chip's undersurface, also leading to a reduction in the cutting forces.
11. The strain hardening of the chips during the application of HPC have a positive impact on their breakability. This is supported by EBSD results, which confirm the presence of highly deformed grain textures.

8. References

- [1] G. Lütjering and J. C. Williams, *Titanium*. Berlin, Heidelberg: Springer, 2007.
- [2] Veiga C., Devim J. P., and Loureiro A. J. R., "Properties and applications of titanium alloys: a brief review," *Rev. Adv. Mater. Sci.*, vol. 32, no. 2, pp. 133–148, 2012.
- [3] A. Umapathi and S. Swaroop, "Mechanical properties of a laser peened Ti-6Al-4V," *Opt. Laser Technol.*, vol. 119, no. August 2018, p. 105568, Nov. 2019.
- [4] V. Wagner, M. Baili, and G. Desein, "The relationship between the cutting speed, tool wear, and chip formation during Ti-5553 dry cutting," *Int. J. Adv. Manuf. Technol.*, vol. 76, no. 5–8, pp. 893–912, Feb. 2015.
- [5] R. M'Saoubi *et al.*, "High performance cutting of advanced aerospace alloys and composite materials," *CIRP Ann. - Manuf. Technol.*, vol. 64, no. 2, pp. 557–580, 2015.
- [6] R. R. Boyer and R. D. Briggs, "The Use of β Titanium Alloys in the Aerospace Industry," *J. Mater. Eng. Perform.*, vol. 22, no. 10, pp. 2916–2920, Oct. 2013.

- [7] C. Paper, S. Pi, and S. Pi, "Comparison of Cutting Tool Performance in Machining of Titanium Alloys and Inconel 718 Super Alloy Comparison of Cutting Tool Performance in Machining of Titanium Alloys and Inconel 718 Super Alloy," no. January 2016, pp. 2–7, 2010.

- [8] Y. Sun, B. Huang, D. A. Puleo, and I. S. Jawahir, "Enhanced Machinability of Ti-5553 Alloy from Cryogenic Machining: Comparison with MQL and Flood-cooled Machining and Modeling," *Procedia CIRP*, vol. 31, pp. 477–482, 2015.

- [9] J. C. Fanning, "Properties of TIMETAL 555 (Ti-5Al-5Mo-5V-3Cr-0.6Fe)," *J. Mater. Eng. Perform.*, vol. 14, no. 6, pp. 788–791, Dec. 2005.

- [10] E. O. Ezugwu, R. Batista Da Silva, W. Falco Sales, and A. Rocha Machado, "Overview of the Machining of Titanium Alloys," in *Encyclopedia of Sustainable Technologies*, vol. 2, Elsevier, 2017, pp. 487–506.

- [11] E. O. Ezugwu, "Key improvements in the machining of difficult-to-cut aerospace superalloys," *Int. J. Mach. Tools Manuf.*, vol. 45, no. 12–13, pp. 1353–1367, Oct. 2005.

- [12] T. Cayli, F. Klocke, and B. Döbbeler, "Increasing Energy Efficiency in Turning of Aerospace Materials with High-Pressure Coolant Supply," *Procedia*

Manuf., vol. 21, pp. 405–412, 2018.

- [13] R. R. Boyer, “Titanium for aerospace: Rationale and applications,” *Adv. Perform. Mater.*, vol. 2, no. 4, pp. 349–368, Oct. 1995.
- [14] I. Inagaki, T. Takechi, S. Yoshihisa, and A. Nozomu, “Application and Features of Titanium for the Aerospace Industry[J],” *Nippon Steel & Sumitomo Metal Technical Report*, no. 106. pp. 22–27, 2014.
- [15] R. R. Boyer, “An overview on the use of titanium in the aerospace industry,” *Mater. Sci. Eng. A*, vol. 213, no. 1–2, pp. 103–114, Aug. 1996.
- [16] A. Ugarte, R. M’Saoubi, A. Garay, and P. J. Arrazola, “Machining behaviour of Ti-6Al-4V and Ti-5553 alloys in interrupted cutting with PVD coated cemented carbide,” *Procedia CIRP*, vol. 1, no. 1, pp. 202–207, 2012.
- [17] F. H. Froes, “Titanium: Alloying,” in *Encyclopedia of Materials: Science and Technology*, Elsevier, 2001, pp. 9361–9364.
- [18] P.-J. Arrazola, A. Garay, L.-M. Iriarte, M. Armendia, S. Marya, and F. Le Maître, “Machinability of titanium alloys (Ti6Al4V and Ti555.3),” *J. Mater. Process. Technol.*, vol. 209, no. 5, pp. 2223–2230, Mar. 2009.
- [19] Q. Zhao, F. Yang, R. Torrens, and L. Bolzoni, “PM versus IM Ti-5Al-5V-5Mo-

3Cr Alloy in Mechanical Properties and Fracture Behaviour,” vol. 22, 2019.

- [20] Z. Wang- and X. Wang, “Mechanical properties of heat treated Ti-5Al-5V-5Mo-3Cr, an attempt to define critical properties of various microstructural features.”
- [21] M. G. E. P. P.J. Arrazola, Ainhara Garay, Irantzu Sacristán, L.M. Iriarte, Dani Soler, “Mecanizado de aleaciones de titanio empleadas en aeronáutica,” *19 Congr. Máquinas-Herramienta y Technol. Fabr. Donostia – San Sebastián*, pp. 1–13, 2013.
- [22] E. O. Ezugwu and Z. M. Wang, “Titanium alloys and their machinability—a review,” *J. Mater. Process. Technol.*, vol. 68, no. 3, pp. 262–274, Aug. 1997.
- [23] C. Leyens and M. Peters, *Titanium and Titanium Alloys*. Köln, Germany: Wiley, 2003.
- [24] M. C. Shaw, *Metal Cutting Principles*, no. 2. New York: Oxford University Press, 2002.
- [25] P. A. Dearnley and A. N. Gearson, “Evaluation of principal wear mechanisms of cemented carbides and ceramics used for machining titanium alloy IMI 318,” *Mater. Sci. Technol.*, vol. 2, no. 1, pp. 47–58, Jan. 1986.

- [26] R. Komanduri, "Some clarifications on the mechanics of chip formation when machining titanium alloys," *Wear*, vol. 76, no. 1, pp. 15–34, Feb. 1982.
- [27] J. D. Puerta Velásquez, B. Bolle, P. Chevrier, G. Geandier, and A. Tidu, "Metallurgical study on chips obtained by high speed machining of a Ti–6wt.%Al–4wt.%V alloy," *Mater. Sci. Eng. A*, vol. 452–453, pp. 469–474, Apr. 2007.
- [28] Y. Kaynak, A. Gharibi, and M. Ozkutuk, "Experimental and numerical study of chip formation in orthogonal cutting of Ti-5553 alloy: the influence of cryogenic, MQL, and high pressure coolant supply," *Int. J. Adv. Manuf. Technol.*, vol. 94, no. 1–4, pp. 1411–1428, Jan. 2018.
- [29] E. M. Trent, *Metal Cutting*, no. 2. London: Butterworths, 1983.
- [30] W. Liu and Z. Liu, "High-pressure coolant effect on the surface integrity of machining titanium alloy Ti-6Al-4V: a review," *Mater. Res. Express*, vol. 5, no. 3, p. 032001, Mar. 2018.
- [31] M. A. Suhaimi, G.-D. Yang, K.-H. Park, M. J. Hisam, S. Sharif, and D.-W. Kim, "Effect of Cryogenic Machining for Titanium Alloy Based on Indirect, Internal and External Spray System," *Procedia Manuf.*, vol. 17, pp. 158–165, 2018.

- [32] K.-H. Park *et al.*, “The effect of cryogenic cooling and minimum quantity lubrication on end milling of titanium alloy Ti-6Al-4V,” *J. Mech. Sci. Technol.*, vol. 29, no. 12, pp. 5121–5126, Dec. 2015.
- [33] Chetan, S. Ghosh, and P. V. Rao, “Comparison between sustainable cryogenic techniques and nano-MQL cooling mode in turning of nickel-based alloy,” *J. Clean. Prod.*, vol. 231, pp. 1036–1049, Sep. 2019.
- [34] A. Khatri and M. P. Jahan, “Investigating tool wear mechanisms in machining of Ti-6Al-4V in flood coolant, dry and MQL conditions,” *Procedia Manuf.*, vol. 26, pp. 434–445, 2018.
- [35] A. Attanasio, M. Gelfi, C. Giardini, and C. Remino, “Minimal quantity lubrication in turning: Effect on tool wear,” *Wear*, vol. 260, no. 3, pp. 333–338, Feb. 2006.
- [36] F. Klocke, D. Lung, T. Cayli, B. Döbbeler, and H. Sangermann, “Evaluation of Energy Efficiency in Cutting Aerospace Materials with High-Pressure Cooling Lubricant Supply,” vol. 15, no. 6, pp. 1179–1185, 2014.
- [37] Z. Fang and T. Obikawa, “Turning of Inconel 718 using inserts with cooling channels under high pressure jet coolant assistance,” *J. Mater. Process. Technol.*, vol. 247, no. March, pp. 19–28, Sep. 2017.

- [38] M. J. Bermingham, S. Palanisamy, D. Kent, and M. S. Dargusch, "A comparison of cryogenic and high pressure emulsion cooling technologies on tool life and chip morphology in Ti-6Al-4V cutting," *J. Mater. Process. Technol.*, vol. 212, no. 4, pp. 752–765, Apr. 2012.
- [39] Z. Bi, *Finite Element Analysis Applications*. London: Elsevier, 2018.
- [40] C. Liu *et al.*, "Benchmarking of several material constitutive models for tribology, wear, and other mechanical deformation simulations of Ti6Al4V," *J. Mech. Behav. Biomed. Mater.*, vol. 97, no. April, pp. 126–137, Sep. 2019.
- [41] A. I. Vakis *et al.*, "Modeling and simulation in tribology across scales: An overview," *Tribol. Int.*, vol. 125, no. November 2017, pp. 169–199, Sep. 2018.
- [42] S. N. Melkote *et al.*, "Advances in material and friction data for modelling of metal machining," *CIRP Ann.*, vol. 66, no. 2, pp. 731–754, 2017.
- [43] S. Berezvai, T. G. Molnar, A. Kossa, D. Bachrathy, and G. Stepan, "Numerical and experimental investigation of contact length during orthogonal cutting," *Mater. Today Proc.*, vol. 12, pp. 329–334, 2019.
- [44] J. Q. Xie, A. E. Bayoumi, and H. M. Zbib, "FEA modeling and simulation of shear localized chip formation in metal cutting," *Int. J. Mach. Tools Manuf.*, vol. 38, no. 9, pp. 1067–1087, Sep. 1998.

- [45] H. Bil, S. E. Kiliç, and A. E. Tekkaya, "A comparison of orthogonal cutting data from experiments with three different finite element models," *Int. J. Mach. Tools Manuf.*, vol. 44, no. 9, pp. 933–944, 2004.
- [46] X. Man, D. Ren, S. Usui, C. Johnson, and T. D. Marusich, "Validation of Finite Element Cutting Force Prediction for End Milling," *Procedia CIRP*, vol. 1, no. 1, pp. 663–668, 2012.
- [47] R. Komanduri and Z. . Hou, "A review of the experimental techniques for the measurement of heat and temperatures generated in some manufacturing processes and tribology," *Tribol. Int.*, vol. 34, no. 10, pp. 653–682, Oct. 2001.
- [48] C. S. Akhil, M. H. Ananthavishnu, C. K. Akhil, P. M. Afeez, R. Akhilesh, and R. Rajan, "Measurement of Cutting Temperature during Machining," *J. Mech. Civ. Eng.*, vol. 13, no. 2, pp. 102–116, 2016.
- [49] P. Hoier, U. Klement, N. Tamil Alagan, T. Beno, and A. Wretland, "Flank wear characteristics of WC-Co tools when turning Alloy 718 with high-pressure coolant supply," *J. Manuf. Process.*, vol. 30, pp. 116–123, Dec. 2017.
- [50] K. A. Jagtap and R. S. Pawade, "Some Studies on Chip Formation Mechanism in CNC Turning of Biocompatible Co-Cr-Mo Alloy," *Procedia*

Manuf., vol. 20, pp. 283–289, 2018.

- [51] S. N. B. Oliaei and Y. Karpap, “Built-up edge effects on process outputs of titanium alloy micro milling,” *Precis. Eng.*, vol. 49, pp. 305–315, Jul. 2017.
- [52] M. S. Dargusch, S. Sun, J. W. Kim, T. Li, P. Trimby, and J. Cairney, “Effect of tool wear evolution on chip formation during dry machining of Ti-6Al-4V alloy,” *Int. J. Mach. Tools Manuf.*, vol. 126, no. December 2017, pp. 13–17, Mar. 2018.
- [53] A. Chandra, P. Karra, A. Bragg, J. Wang, and G. Y. Kim, “Chip Segmentation in Machining: A Study of Deformation Localization Characteristics in Ti6Al4V,” in *Volume 1: Processing*, 2013.
- [54] V. A. Bykov, T. V. Kulikova, L. B. Vedmid’, A. Y. Fishman, K. Y. Shunyaev, and N. Y. Tarenkova, “Thermophysical properties of Ti-5Al-5V-5Mo-3Cr-1Zr titanium alloy,” *Phys. Met. Metallogr.*, vol. 115, no. 7, pp. 705–709, 2014.
- [55] J. D. Cotton *et al.*, “State of the Art in Beta Titanium Alloys for Airframe Applications,” *Jom*, vol. 67, no. 6, pp. 1281–1303, 2015.
- [56] Y. Yuan, X. Jing, K. F. Ehmann, J. Cao, H. Li, and D. Zhang, “Modeling of cutting forces in micro end-milling,” *J. Manuf. Process.*, vol. 31, pp. 844–858, Jan. 2018.

- [57] A. Gómez-Parra, M. Álvarez-Alcón, J. Salguero, M. Batista, and M. Marcos, "Analysis of the evolution of the Built-Up Edge and Built-Up Layer formation mechanisms in the dry turning of aeronautical aluminium alloys," *Wear*, vol. 302, no. 1–2, pp. 1209–1218, Apr. 2013.